

Shape memory polymer-based smart plug for inguinal hernia repair

by

Muhammad Bilal

A thesis submitted in partial fulfillment of the requirements for the degree of

Master of Science

Department of Mechanical Engineering

University of Alberta

© Muhammad Bilal, 2021

## **Abstract**

The application of hernia meshes is amongst the most popular techniques used to treat and repair hernias worldwide. While there is no gold standard at this point, the conventional technique involves repositioning of the displaced tissue back into the desired location followed by the application of a hernia mesh which is secured in place by either sutures, stitches, or adhesives. This is critical to ensure that the previously displaced tissue remains in its allocated position, giving the body sufficient time to heal and alleviate reliance from the mesh. In contrast to conventional meshes, 3D meshes have proven to provide a more sustainable recovery pathway for patients and has gained significant traction by the medical community. Given the advantages of 3D meshes over conventional meshes, such as increased motility, reduced pain, reduced scarring as well as increased rate of recovery, this study proposed a new design of a 3D hernia scaffold using a smart material, namely shape memory polymer (SMP). Unlike conventional static meshes which require intricate surgical precision and accuracy to ensure the complete placement of the mesh, the proposed design in this study displays self-deployment capabilities, which is based on shape memory effect (SME), upon activation. Once the device is transferred to the site of the hernia, the self-deployment of the proposed model is achieved by thermal activation, at normal human body temperature, expanding to its full size and gripping the site without the need of sutures with the adjacent tissue to support it. The self gripping nature of the proposed design has the potential to reduce the time and complexity of the hernia repair surgery with the added benefits offered by 3D meshes. The present study compared a multitude of designs based on a design selection criterion including ease of printing, repeatability, design constraints and functionality. After several iterations, a single design was proposed, 3D printed, and then tested to determine mechanical and shape memory properties. The mechanical properties, of the proposed design, were investigated

by analyzing the effect of static compressive forces and cyclic compressive forces on 3D printed samples and comparing them to equivalent data found in literature for existing commercial alternatives. The results of the static compression test indicated that the proposed design displayed a maximum force of 18.74 N/cm without signs of failure, conforming to its commercial counterparts which display a range of 11.1 N/cm to 100.9 N/cm before failure. The stiffness parameter for the proposed design was determined in this study to be 1.58 N/mm which is also comparable to the available commercial alternatives exhibiting a range of 0.3 N/mm to 4.6 N/mm. The results of the cyclic compression test displayed a higher plastic deformation of 14.67% in comparison to the range of 0.58% to 8.51% demonstrated by the commercial alternatives compared in this study. These differences were considered acceptable and did not invalidate the effectiveness of the proposed design since this was an indirect comparison and minor differences were expected. The shape memory properties were studied by analyzing the smart plug deployment under controlled conditions to determine the speed of recovery as well as the recovery ratio. While no comparison can be made against a commercial hernia mesh for these shape memory properties, the samples showed shape recovery of more than 90% within four minutes of activation which is a quite promising difference than current surgical procedure time. Due to the ongoing COVID-19 restrictions and laboratory closures, this study experienced significant delays with both the speed of the project and deliverables being affected.

## **Acknowledgements**

This thesis has led me on an amazing journey with challenges and opportunities at every corner. It has been an absolute honour and privilege for me to be a part of this journey with the relentless support, guidance and patience of Dr. Cagri Ayranci and Dr. Ahmed Qureshi. With moments of doubt and uncertainty, they guided me to a place of more confidence and conviction, helping me to achieve this milestone. I would also like to thank Dr. Irina Graces who not only provided mentorship throughout this thesis but also with critical insight based on her experience without which this journey would have been significantly more challenging. I would like to also thank Dr. Omar Farooq for offering his medical expertise in this matter and proactively ensuring the success of this study to the best of his abilities.

Last but never least, I would like to thank my parents for their never-ending support, love, patience and assurance during this journey. They have unknowingly been my constants in life without which this study would not have been possible. I would also like to thank my sister for her absolute confidence in me which always led me to work harder to ensure the success of this study. I would also like to thank my fiancé for the faith placed in me, for the love, support and guidance offered to me during these trying times.

# Contents

<b>CHAPTER 1: INTRODUCTION TO THESIS .....</b>	<b>1</b>
1.1 MOTIVATION .....	1
1.2 THESIS OBJECTIVE .....	4
1.3 THESIS OUTLINE .....	4
<b>CHAPTER 2: LITERATURE REVIEW .....</b>	<b>6</b>
GAP IN LITERATURE AND MOTIVATION .....	15
<b>CHAPTER 3: METHODOLOGY .....</b>	<b>18</b>
3.1 DESIGN PHASE .....	18
3.2 FABRICATION PHASE .....	32
3.3 CHARACTERISATION PHASE.....	39
3.3.1 <i>Mechanical Characterisation</i> .....	39
3.3.2 <i>Shape Memory Characterization</i> .....	43
<b>CHAPTER 4: RESULTS &amp; DISCUSSION.....</b>	<b>48</b>
4.1 MECHANICAL CHARACTERIZATION .....	48
4.1.1 <i>Compression Testing</i> .....	48
4.1.2 <i>Cyclic Compression Test</i> .....	52
4.2 SHAPE MEMORY CHARACTERISTICS .....	54
<b>CHAPTER 5: CONCLUSION AND FUTURE WORKS .....</b>	<b>58</b>
<b>BIBLIOGRAPHY.....</b>	<b>61</b>

## List of Tables

Table 1: Summary of key design features for smart plug.....	31
Table 2: Summary of Extrusion Heating Zone Temperatures for Extruder .....	37
Table 3: Summary of printing parameters .....	38
Table 4: Summary of results for single compression test.....	51
Table 5: Mechanical properties of commercial alternatives [61] .....	51

## List of Figures

Figure 1: ProFlor by Insightra - Picture adopted from Insightra.com .....	11
Figure 2: Ethicon Prolene J&J .....	12
Figure 3: Ethicon Ultrapro (UHSL6) J&J.....	12
Figure 4: Pre-activation design schematic .....	18
Figure 5: Post-activation design schematic.....	19
Figure 6: First Design Iteration.....	21
Figure 7: CAD model for second design iteration .....	22
Figure 8: 3D printed sample for second design iteration .....	23
Figure 9: CAD model for third iteration.....	23
Figure 10: 3D printed sample for third design iteration .....	23
Figure 11: Shape memory programming of third design iteration .....	24
Figure 12: Waist endcap deformation.....	25
Figure 13: CAD model for fourth iteration.....	26
Figure 14: 3D printed sample for fourth design iteration .....	26
Figure 15: Programming attempt for a 3D printed sample of the fourth design iteration .....	27
Figure 16: Common defects in 3D printed sample of fourth design iteration .....	28
Figure 17: CAD Model of final design iteration with supports .....	29
Figure 18: CAD Model of final design iteration without supports.....	29
Figure 19: Comparison of 3D printed sample between final design iteration with fourth design iteration .....	29
Figure 20: Print results of final design iteration using optimised print parameters.....	30
Figure 21: Vacuum Oven - Lindberg/Blue M from Thermo Fisher Scientific Inc.....	35
Figure 22: Brabender™ single screw extruder .....	36
Figure 23: Drive system to wind filament .....	36
Figure 24: Schematic of Inguinal Hernia.....	40
Figure 25: Schematic of conventional mesh attached to hernia site .....	40
Figure 26: Bose ElectroForce 3200 Series 3 test instrument.....	42
Figure 27: Sample before compression.....	42
Figure 28: Sample after compression .....	43
Figure 29: Pre-activation Image recording activation .....	45

Figure 30: Post-activation Image recording activation.....	45
Figure 31: Pre-activation image recording activation with tracking points.....	46
Figure 32: Post-activation image recording activation.....	47
Figure 33: Force versus Displacement graph for all samples.....	49
Figure 34: Model calculation for single compression test.....	50
Figure 35: Plastic deformation under cyclic loading.....	53
Figure 36: Activation comparison of short overhangs.....	55
Figure 37: Activation comparison of long overhangs.....	55
Figure 38: Recovery comparison of short vs long overhangs.....	56
Figure 39: Activation comparison of waist.....	56

## **Glossary of Terms**

**2D** Two Dimensional

**3D** Three Dimensional

**SMP** Shape Memory Polymer

**SMPU** Shape Memory Polyurethane

**SME** Shape Memory Effect

**SMA** Shape Memory Alloy

**CAD** Computer Aided Design

**IAP** Internal Abdominal Pressure

**FDM** Fuse Deposition Modeling

**UM3** Ultimaker 3 (3D Printer)

**MM4520** Thermoplastic polyurethane-based shape memory polymer

**PVA** Polyvinyl Alcohol

# Chapter 1: Introduction to Thesis

## 1.1 Motivation

Hernias are a prevalent and ongoing disease that affects millions of men, women, and children globally. With efforts directed to improve current practices and conduct hernia repair procedures and surgeries, the hernia industry is now focused on the development of innovative designs and improved technology to reduce patient pain, complication rate and procedure complexity. While there is no definitive standard, typical hernia repair procedures involve the use of conventional meshes that are secured at the hernia site by means of sutures, tacks, or adhesives. These conventional meshes, which are referred to as static meshes in some instances in the literature and are 2D in shape, push the protruded tissue or hernia back in the desired location effectively repairing the hernia [1] [2]. While the use of synthetic conventional meshes is the popular technique utilized to conduct hernia repair surgeries it is not without its flaws. These conventional meshes have a high rate of recurrence, are known to cause pain in patients and are also reported to result in medical complications [3]. The use of conventional meshes also results in poor quality of tissue regrowth and is often associated with tearing and bleeding at the hernia site [3]. Recent innovations in these conventional meshes includes the use of lighter materials to reduce the weight of meshes reducing the foreign body reaction by the human body, which in turn results in lower pain experienced by the patient [4]. Investigation into the use of larger pore size has also resulted in higher dynamic movement as well as lower probability of infection which in turn reduces the chances of tearing and medical complications [5][6]. While there has been significant work on the mechanical, material and structural properties to improve these desired properties, synthetic conventional meshes still face inherent challenges that have not been addressed by these improvements. The foreign body reaction caused by the use of sutures, tacks or adhesive to secure

the mesh in the hernia site is reported to contribute to the complication rate in hernia repair procedures [3]. The use of various 3D meshes (Figure 1) have proved to be excellent alternatives addressing the inherent issues faced by these conventional meshes and are reported to have a superior quality of tissue regrowth as well as lower pain experienced by the patient [7]. With the obvious advantages of 3D meshes over conventional (2D) meshes, significant effort has been directed to further develop this technology to leverage the advantages offered by the new designs. Despite this, the integration of shape memory polymers (SMPs) has remained absent in the development of 3D meshes. SMPs integrated in conventional meshes have reported to yield faster deployment reducing procedure time and complexity but have still maintained the inherent issues faced by all conventional meshes. With the potential advantages of the use of 3D meshes over conventional 2D meshes, and the added advantage of reduced procedure complexity and time, this research aims to deliver a proof of concept (prototype), introducing a novel design and self-deploying capabilities using smart materials. Based on SMPs, the current design aims to be compatible with the more popular and less invasive laparoscope assisted hernioplasty providing a faster deployment compared to existing 3D meshes while leveraging on their existing advantages over conventional static meshes. The proposed smart plug is required to fit in a 10 mm tube (Figure 2) similar to that of a laparoscope and once inserted and pushed into the body, expanding to 50 mm diameter (Figure 3) due to thermal activation, effectively sealing the weakened cavity. To achieve these requirements some fundamental research questions needed to be formulated that this study would address.

- What would be the appropriate shape or structure that could achieve the requirement of morphing from its regular size (50 mm) to fit inside a laparoscopic tube (10 mm) and then

redeploy back into its regular size, also defined as “functional requirement” later in this study?

- Which type of materials are used to make hernia repair meshes and which materials could achieve this functional requirement?

Such as device needed to have sufficient strength to survive inside the abdominal cavity and it was important to know what the commercial benchmark was and where our proposed device stands.

- What commercial alternatives are available along with their mechanical properties? What are the mechanical properties of our proposed design that could be compared with existing alternatives?
- How could the functional requirement be characterized and compared with existing alternatives to conclude if they were acceptable?

These research questions form the crux of this study and were the foundation of the research objectives of this study. The scope of this study includes the complete design, fabrication using shape memory polymers, mechanical and shape memory characterisation. Therefore, this study is divided into three main sections: the design phase, the fabrication phase, and the characterisation phase. The design phase involved a series of iterations that were performed to achieve the final design keeping in mind important considerations including but not limited to functionality, ease of fabrication and repeatability. The fabrication phase of this study involved determining and implementing the appropriate technique required to fabricate a working prototype and define the optimal parameters that would ensure fabrication repeatability. Upon successful fabrication and test of functionality, the characterisation phase of this study aimed to determine its key mechanical and shape memory characteristics while making a comparison between the smart plug with

existing data found in the literature. This phase was crucial in determining the validity of the research objective.

## 1.2 Thesis Objective

Keeping in mind the research questions posed earlier, the aim of this study was to develop a 3D alternative to the conventional meshes, that are used in hernia repair procedures, with shape memory properties that would activate upon insertion at the hernia site via a laparoscope or similar device while addressing the research questions simultaneously.

Keeping this in mind, the objectives of the research are:

- To deliver a functional prototype of a smart plug that can be used for hernia repair surgeries as a proof of concept.
- To characterise the mechanical and shape memory characteristics of the prototype experimentally
- To provide an analysis of validity of the smart plug to determine its potential application

To achieve these objectives, a single design was selected out of multiple possible concept designs and fabricated while ensuring acceptable quality and functional requirements. The samples for this selected design were then characterised to determine their mechanical and shape memory properties and compared with existing commercial alternatives to determine the effectiveness of the proposed design.

## 1.3 Thesis Outline

This thesis is organised into five chapters. The second chapter of the thesis introduces some important terminologies and a data driven argument to show the impact caused by hernias as well as details of some commercially used products, and their properties, which were used for

comparisons throughout the study. Finally, the second chapter discusses some important concepts such as shape memory polymers that were critical in the application of this study.

The third chapter of the thesis discusses the design criterion used to develop the 3D scaffold as well as a walk-through of the different design iterations and the justification of the current design, and its features, against previous iterations. It also discusses the fabrication process that was employed along with the materials and equipment used. The last section of this chapter discusses the methodology and set-up of the mechanical and shape memory tests that were conducted to investigate the properties of the 3D hernia scaffold.

The results of the tests and discussion on these results, and their comparison to commercially available products are discussed in the fourth chapter. The fifth chapter of this study concludes this thesis with comments about future work and limitation about this study.

## Chapter 2: Literature Review

A hernia is defined as the protruding of an internal organ or other body part through either a muscular or tissue wall that normally contains it [8]. While the term “hernia” is a relatively broad term and may be classified into further sub-categories depending upon the location of the hernia including but not limited to femoral hernias which occur at top of the inner thighs, umbilical hernias near the navel and hiatal hernias located on the chest through the diaphragm. Inguinal hernia occurs when a fatty tissue or part of the intestines protrude into the groin through a weakened tissue wall, which is normally meant to restrict it in place, at the top of the inner thigh. This type of hernia is quite common and affects both men and women [8] [9] [10]. With an estimated case-load of 20 million inguinal hernia repairs worldwide annually, it is estimated that the lifetime risk for men and women is 27% and 3%, respectively [11]. While majority of these surgeries tend to proceed smoothly with no complications, one study reported a 5% complication rate. 15% of patients in this study also reported pain and discomfort after the first 24 hours of the surgery [12]. A similar study reported an overall complication rate of 19.5% out of which major complications, including pulmonary and cardiovascular, accounted for 15.1% of the total complication rate [13]. Typically after such a procedure, patients are discharged within 24 hours and are able to return to leisure activities and work on an average of 3.1 to 5.6 days [12]. While the time to return back to leisure activities is acceptable given the current hernia repair methods and techniques available, it has a significant margin to be reduced while also reducing the complexity and complication rate of the procedure.

With the prevalence of hernia cases and complications presented, the hernia repair industry is projected to transition from USD 4.09 billion from 2018 to USD 4.75 billion by 2023. The increased acceptance and implementation of conventional meshes in hernia repair surgeries is

considered a major driving factor for this projected increase. Recent innovations made to conventional meshes including but not limited to biological meshes have also shown promising growth and projections while reducing potential issues that that are faced by conventional meshes [14] .

With the absence of a universally accepted “gold standard” in the hernia repair industry, several techniques have made their way as good practices to characterize the treatment of this disease. The main techniques employed include the use of commercially available prosthetic which may be further classified into static, and dynamic meshes. Static and dynamic meshes, in terms of hernia repair devices, are categorized based on their ability to move with the abdominal wall and accommodate the motility of the abdomen. Static meshes are fixed to the abdominal wall by means of sutures, tacks or adhesives and do not accommodate the movement of the abdominal wall. While dynamic meshes may also be fixed to the abdominal wall similarly, their structure has sufficient tolerance to allow for the natural motion of the abdominal wall and resists tears to higher degree [3]. The use of conventional meshes, which are classified under static devices, is not mandatory and surgeons may also opt to perform a “tension repair”, where an abdominal incision is made over the hernia site and the protruding tissue is pushed back into its normal location. The surgeon then directly stitches the edges of the defect using multiple sutures as required [1]. While this technique may seem straightforward, it has a been discarded in most developed countries due to the high recurrence rate and post-operative pain experienced by patients. The “tension-free repair” has since replaced this technique and requires the use of synthetic static or fixated meshes in the location of the hernia site, after which the surgeon sutures around the circumference of the defect without sewing the defect shut. This technique offers the advantage of avoiding the application of pressure on the muscular tissue surrounding the defect, which could potentially weaken the region

further [10] [11]. The use of prosthetics, including meshes, provides the advantages that tension free repair offers however this technique requires surgeons to open the abdominal wall to place and secure the mesh. An improvement made to this technique by Lablanc and Booth [16] further reduced the complexity of this procedure by introducing the mesh directly into the abdominal cavity by using a minimally invasive technique via a laparoscope. The adaptation of this technique is more frequently performed, and is generally associated with lower pain, lower recurrence rate and a faster recovery. While the difference between both techniques is beyond the scope of this study, both techniques, however, support the use of meshes as being the acceptable way forward [17] .

With the use of meshes being in the centre of hernia repair surgeries, the race to innovate this technology is mainly focused towards either design adaptations, in an attempt to fix the inherent challenges posed by all types of conventional meshes, or material optimisation to improve certain desired properties. These desired properties can be categorised as material properties, structural properties, and mechanical properties. The selection of materials strongly influences the inflammatory response of the body which in turn determines recovery rates as well as pain experienced by the patient [5][18][19][20]. The structural properties can be further subcategorised into pore characteristics and weight of the mesh. The pore characteristics play a critical role in influencing the limited dynamic movement of the mesh, which is caused by the collapse of the pores under strain [5]. Mesh porosity is also a determining factor for the risk of infection [6]. The weight of synthetic meshes can be used to classify meshes as either lightweight or heavyweight depending upon the polymer weight and amount of raw material used. Lightweight meshes have a weight per unit area ranging from 35 to 70 g/m<sup>2</sup>, standard weight meshes from 70 to 140 g/m<sup>2</sup> and heavyweight meshes being greater than 140 g/m<sup>2</sup> [21] . Since lightweight meshes contain less

material than their counterparts, they induce a moderate foreign body reaction in the body with decreased inflammatory response providing better tissue incorporation, reduced patient discomfort and increased prosthesis acceptance, providing a notable advantage over heavyweight meshes [4]. While the mesh weight does not influence the rate of reoccurrence, patients with lightweight meshes have reported lower discomfort and an earlier return to activity as compared to heavyweight meshes [22][23]. With all these advantages, however, lightweight meshes exhibit lower tensile strength as well as a lower burst strength in comparison to heavyweight meshes [24][25]. These mechanical properties are critical in determining the suitability of a particular mesh for its appropriate clinical application.

Tensile strength, burst strength and stiffness are some of the major mechanical properties which are considered while designing meshes. While tensile strength is conventionally defined as the maximum force that can be applied before failure per unit area, for the purpose of meshes, it is usually reported in relations to clamping width with units usually being N/cm or equivalent [5]. The burst strength is defined as the maximum uniformly distributed pressure applied at a right angle to the surface of a material to withstand standardized conditions [26]. Due to the difference in shape as well as loading conditions, as explained in Chapter 3 (3.3.1) of this study, between our proposed design in contrast to conventional meshes, the burst strength was not applicable for our case and was disregarded. Stiffness is defined as the ability of a material or object to resist deformation and can be calculated as the slope of the force versus displacement curve [27]. Stiffness was critical in our application since a significant difference in stiffness between a mesh and the abdominal wall could cause discomfort to the patient. Meshes with higher stiffness tend to dehisce from the abdominal wall when the patient moves [28].

It is important to note that a large proportion of commercially available synthetic meshes are designed based on these mechanical properties are made from select materials including but not limited to Polytetrafluoroethylene (ePTFE), polypropylene (PP), polyethylene terephthalate (PET) and polyvinylidene fluoride (PVDF), providing improved mechanical strength, including higher tensile strength as well as burst strength, at a lower cost [5][29].

With the general acceptability of the use of synthetic static meshes or fixated meshes due to their advantages as well as convenience, there are some inherent problems with the use of static synthetic meshes that have gradually been identified. The typical biological response due to the application of conventional meshes does not represent the tissue regeneration but rather a foreign body reaction mainly caused by the fixation mechanisms used to hold the mesh in place, which in turn is correlated to high complication rate of hernia repair surgeries [3]. The treatment of inguinal hernias with the application of static synthetic meshes are not entirely tension free and is associated with tearing, bleeding, hematoma as well as nerve entrapment which not only result in mesh dislocation but also poor quality of tissue regrowth [30]. This produces a rigid fibrotic scar plaque causing severe discomfort and pain, instead of regenerating the weakened tissue, which is the root cause of the problem, and should be the target [31][32]. With this consideration as well the fact that the groin region is one of the most motile regions of the body and is subject to constant motion, the development of 3D meshes was considered as a reasonable solution to this inherent problem. A self-retaining 3D implant (ProFlor), developed by Amato et al. and commercialized by Inshightra as shown in Figure 1, fits into place using centrifugal expansion without the need of additional anchors for fixation and displays excellent compliance to the dynamic motion that is absent from static meshes [30].

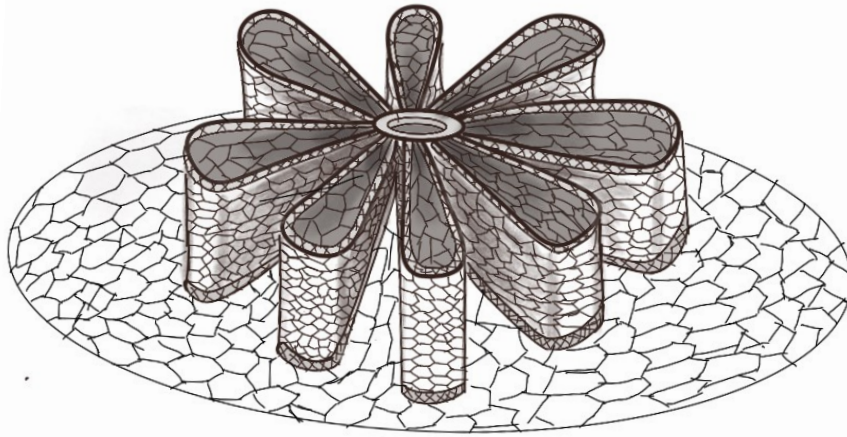


*Figure 1: ProFlor by Inshitra - Picture adopted from Inshitra.com*

A clinical study conducted by Amato et al. to determine the impact of using the ProFlor 3D mesh reported a reduction in post-operative pain and minimized overall complication rate as well as an absence of long-term chronic pain and patient discomfort [3]. Another study conducted by Amato et al. aimed to determine the degree of angiogenesis with respect to time by using ProFlor reported a progressive development of artery and vein infrastructure with time therefore confirming high biological ingrowth due to the use of this prosthetic. The growth of a broad network of arteries and veins is crucial for healthy tissue regeneration which requires significant vascular development [7]. Similar 3D meshes such as the “3D Max mesh” has also shown promising outcomes in comparison to ordinary meshes, effectively reducing operation time as well as decreasing post-operative and chronic pain [33]. With the potential advantages offered by 3D meshes as compared to conventional 2D meshes, a new wave of innovation has been directed in an effort to further reduce the complications of the hernia repair surgery with the use of designs that are evident by the works of Amato et al. and other notable 3D meshes including the 3D max mesh and other promising commercial products such as “Prolene” and the “Ultrapro (Model: UHSL6)” both by Ethicon, Johnson & Johnson, shown in Figure 2 and 3 respectively [32][33].

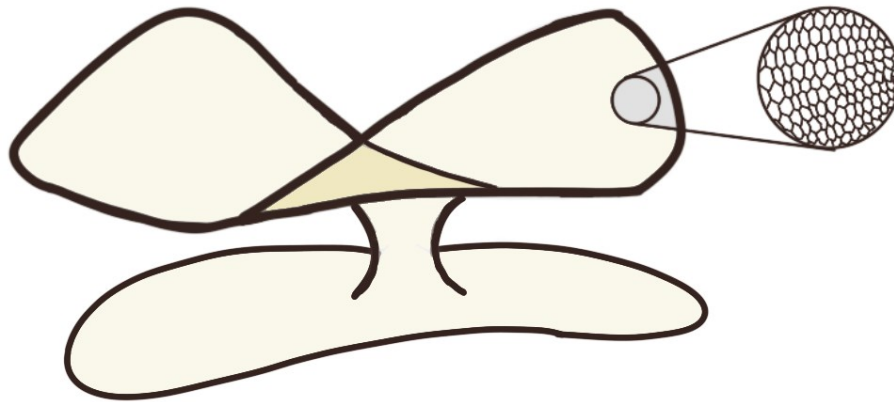


Figure 2: Ethicon Prolene J&J

Picture adopted from - <https://www.jnjmedicaldevices.com/en-US/product/prolene-polypropylene-hernia-system>

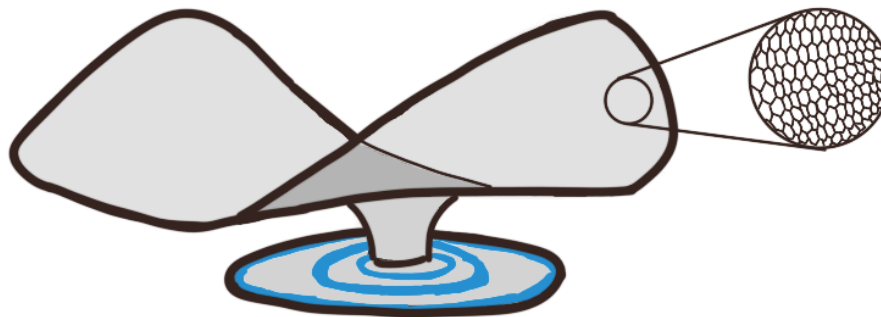


Figure 3: Ethicon Ultrapro (UHSL6) J&J

Picture adopted from - <https://www.ethicon.com/na/epc/code/uhs16?lang=en-default>

While research and innovation into these meshes are far from over, we have yet to see the integration of these 3D meshes with smart materials which are known to provide significant advantages to existing technology, especially in the biomedical field. Smart materials can change physical properties such as shape, colour and size in response to external stimulus [36]. Smart materials have been widely used commercially to develop critical biomedical technology including self-expanding stents for cyanotic patients with congenital heart disease [37][38][39]. Smart materials have also been used to make entire transcatheter heart valves including the leaflets and support structure which can be delivered into the heart using a non-invasive surgery [40]. While the literature is filled with an exhaustive list of applications and advantages for the integration of

smart materials, this study was inclined towards the use of a particular category of smart materials namely shape memory polymers (SMPs).

SMPs are a special branch of materials that display the shape memory effect (SME), which is defined as the ability of such a material to recover from a temporarily assigned shape to its original shape in response to a particular stimulus such as heat, electricity, stress, light, moisture, etc. [41][42]. SMPs that activate on thermal stimuli are the most common type of SMPs and are the basis of this study [43].

These thermo-responsive SMPs are generally categorised in two main groups: thermosets and thermoplastics. Polyurethane based thermoplastic SMPs are quite popular in the literature with their advantages ranging from ease of processing, ability to display excellent SME as well as being light weight. Shape memory polyurethanes (SMPUs) are thermoplastic and can be heated above a certain temperature to be reprocessed and given different shapes, multiple times. The crystalline regions of the SMPUs are hard and brittle in nature, maintaining these characteristics at temperatures below the melting temperature while the amorphous regions are soft and only display these characteristics below the glass transition temperature ( $T_g$ ). Beyond the  $T_g$  but under the melting temperature, the amorphous region transitions from a glassy to rubbery state, making it softer and more flexible while the crystalline region remains in the glassy state. This allows the elastic modulus of the amorphous region to reduce and the SMPU is able to be transformed to a temporary shape. This shape may be fixed if the temperature is cooled to under the  $T_g$  and the appropriate constraints are applied to prevent the temporary shape from changing. The reduction of temperature under the  $T_g$  results in the amorphous region returning to its glassy state. Heating above the  $T_g$  after the temporary shape is programmed, will cause the structure to retain its original shape because of the elastic energy stored in the crystalline region of the SMPU, as the amorphous

region softens and is unable to retain the temporary shape. It is important to note that the amorphous regions are responsible for retaining the temporary shape while the crystalline regions are responsible for retaining the permanent or original shape [44][45].

This study aims to leverage the advantages offered by SMPs including but are not limited to being light weight, processing ease as well as higher recovery strain, which will prove significantly advantageous for the purpose of this study [46]. Due to their ability of recovery to pre-programmed shape upon controlled heat activation, SMPs present a unique opportunity to infiltrate the hernia repair industry [47]. With broad research efforts being directed towards the implementation of SMPs in the bio-medical field including the embolization of aneurysms [48], extraction devices for the treatment of blood clots [49] , as well as the development of cardiovascular stents [50] , it is evident that biomedical application of SMPs has gained significant traction. The use of SMPs has also been applied to develop self rolling meshes intended for hernia repair surgeries aiming to reduce operation time and complexity [51].

## Gap in Literature and Motivation

The literature has abundant instances of the use of SMPs in bio-medical applications, with notable efforts made especially towards the development of cardiovascular stents conducted by Kim et al., Wache et al and Chen et al [50] [52] [53]. While the utility of SMPs for the development of biomedical applications has gained significant traction, the integration of SMPs in the development of hernia repair meshes has only one instance in the literature in the work of Zimkowski et al. Their work involved the integration of SMPs to hernia repair meshes with self unrolling capabilities that are activated by the human body temperature. Their study reported the fastest deployment time of 33 seconds to unroll the mesh. The work posed by Zimkowski et al. [51] provides a promising alternative to existing conventional meshes and justifies further investigation. Since their work focuses on reducing surgical time and complexity, it does not address the inherent issues that are experienced by the use of static synthetic (conventional) meshes, in such a motile area of the body, which leads to higher scar tissue, inflammation and pain experienced by patients [3]. While this particular concern was addressed in the design proposed by Amato et al. [3], shown in Figure 1 of a 3D self gripping mesh, the integration of SMPs in their work was absent. The design presented in their study was developed keeping in mind the inherent issues faced by conventional meshes and aimed to produce a device which improved patient pain, overall complication rate and remove the requirement to secure the device by means of sutures, tacks, and adhesives. The device presented by Amato et al. (ProFlor) is considered to be self gripping which is a feature that is not shared by its counterparts available commercially. Concerns regarding the use of conventional meshes, such as the use of 3D design to accommodate increased motility are addressed by a number of commercial alternatives including but not limited to Ethicon Prolene and Ethicon Ultrapro (UHSL6), shown in Figure 2 and 3 respectively. However, both these

alternatives do not address the operating times and procedure complexity which may be addressed by the incorporation of SMPs as shown in the work of Zimkowski et al. It is also important to note that both these meshes require external mechanisms such as sutures or tacks to secure them which in turn is known to contribute to inflammation and discomfort experienced by the patient.

Conventional (static) meshes are known to have higher recurrence rate and pain experienced by patients due to their shape as well as securing mechanisms, which a complex surgery. While 3D meshes like Ethicon Prolene and Ultrapro (UHSL6) address the concern regarding shape, they fail to address both procedure complexity as well as the impacts such as poor tissue recovery, bleeding and further medical complications caused by securing mechanisms such as sutures, tacks and adhesives. The device proposed by Amato et al. (ProFlor), addressed the concern regarding shape as well as those caused by securing mechanisms by introducing a self gripping design. Their work also proves the resulting improved tissue growth and recovery in their investigation to study the angiogenesis in the vicinity of the hernia site, after using ProFlor compared to conventional meshes [7]. While their work is a notable achievement, paving the way for 3D meshes as the path forward in hernia repair meshes, the procedure complexity still remains quite intricate and time consuming. The work of Zimkowski et al, did however address the issue of procedure complexity and failed to address the other key concerns of conventional meshes discussed.

In light of this information, and due to the limited instances of self-gripping 3D meshes in literature as well as the absence of SMP integration with these meshes, research into new design which addresses all of these concerns was crucial. Such a design was required to be self gripping to avoid the use of external securing mechanisms while possessing the comparable motility to the abdominal wall by use of 3D design. The design must also address surgical time and complexity which could be achieved by the incorporation of SMPs. All this must be achieved while ensuring

practicality of device, ease of use, low cost of production as well as provide easy modification for people of all ages, genders, and sizes. This is the motivation behind the development of a SMP based 3D smart plug that could address all of these concerns.

## Chapter 3: Methodology

### 3.1 Design Phase

The design phase of this study presents all of the steps taken to design the smart plug, including specifying the device requirements, design selection criteria, functional requirements and the various design iterations that were developed and disregarded due to the design selection criteria, that will be discussed later in this Chapter.

The design requirements defined the size constraints that were expected to be met in order for the device to be successfully transported to and implanted in the hernia site. The design requirements of the smart plug can be further sub-categorised into two main sections: Pre-activation and post-activation requirements. The pre-activation shape of the smart plug must be able to fit inside a 10 mm cylindrical tube similar to that of a laparoscope through which it may be transferred to the location of the hernia site. While laparoscopes are available in a variety of sizes including but not limited to 3 mm, 5 mm, and 10 mm, with different manufacturers offering a multitude of sizes, the 10 mm size is widely used for hernia repair surgeries and was considered as the base design dimension for the pre-activation size and can be visualised below in Figure 4.

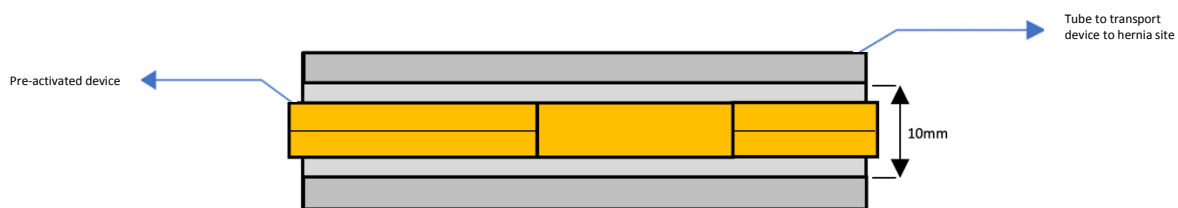
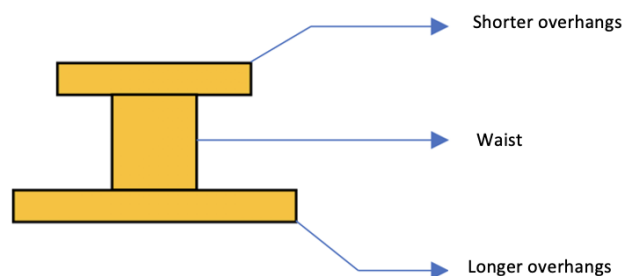


Figure 4: Pre-activation design schematic

The post-activation shape needed to be carefully designed to ensure that the smart plug would be self-gripping, locking itself in place upon deployment effectively blocking the protruding tissue from entering the inguinal canal. To ensure the functionality of the self-locking mechanism, smart plug was required to deploy with three distinct features. The first feature was a set of overhangs

that would face the abdominal cavity. The second feature was a central waist that would allow for expansion from the pre-activation to the post-activation shape. The post-activated waist also needed to have a wider diameter to ensure contact with the weakened tissue in order to increase grip and reduce play that could otherwise be caused. Due to this reason, the waist was required to have an allowance to accommodate for change in diameter. The third feature was a second set of overhangs on the other side of the waist that would face the inguinal canal. The overhangs on either side of the waist would be responsible for locking the smart plug, in place, while obstructing the tissue to move through the weakened wall. Due to the availability of space in the side of the abdomen, the overhangs were designed to be slightly longer, referred hereafter as longer overhangs, compared to the overhangs that face the inguinal canal which are slightly shorter in length due to the space constraint, referred hereafter as shorter overhangs, and can be observed in the final design. The post-activation design can be seen below in Figure 5 which contains a schematic of general requirement.



*Figure 5: Post-activation design schematic*

The shorter overhangs were designed to expand to 30 mm in diameter in contrast to the longer overhangs which can reach 50 mm. These dimensions were an approximation provided by Dr. Omer Farooq, based on his years of surgical experience performing hernioplasties. These dimensions can also be verified by those of “ProFlor” which comes in two sizes, the first being 25

mm and the second being 40 mm, proving that the dimensions implanted in this study are in the vicinity of similar commercial products and therefore valid [53].

The smart plug was then designed and fabricated with reference to the post-activation shape in consideration while ensuring that adequate accommodation was set in place to attain the pre-activation shape. The ability of a particular design iteration to successfully transform from the pre-activation shape (temporary shape) to the post-activation shape (permanent shape) was defined as the functional requirement and deemed critical for a particular design iteration to be considered acceptable.

Once a concept design was developed, it was tested against the design selection criteria which contained four key benchmarks which needed to be fulfilled in their entirety, in order for the design to be finalised and ready for fabrication.

The design selection criteria, including the four key benchmarks were defined as the ability of a particular design to:

- fulfil the functional requirement
- printability or ease of fabrication
- repeatability of fabrication
- design complexity

Any design iteration that did not fulfil even a single benchmark was discarded and modified to ensure compliance to the desired requirements. If that a particular design was successfully fabricated but was unable to satisfy the functional requirement, it was discarded due to its failure to perform the most fundamental requirement which was to change its shape from the pre-activation to the post activation shape. This was a critical requirement for the desired application and could not be foregone. If a design was able to successfully satisfy all other benchmarks but

could not be easily fabricated, then this would create significant problems for future implementation and was subsequently avoided to ensure that future work on this study could be performed without causing hinderance. Fabrication repeatability was critical to ensure successful mechanical and shape memory characterization which, if not achieved, would void the entire research objective. Lastly, the design complexity was critical since it strongly influenced printability, repeatability as well as the functional requirement. A more complex design made fabrication more difficult while significantly reducing the quality of the prototype. If the fabricated product had poor quality, then multiple copies made from the same design would have significant variations between them resulting in potential inconsistencies during the mechanical and shape memory characterisations. A more complex design could, potentially, also make activation and programming the shape memory effect more complex which was not beneficial. Therefore, an acceptable design was outlined to be easy to fabricate, have a simple design, display acceptable repeatability of fabrication, and attain the functional requirement.

While there were a number of design iterations, some of the important designs will be discussed in this study along with the appropriate justifications. The first design iteration of the smart plug can be seen in Figure 6 which shows a series of alternate views for the same design.

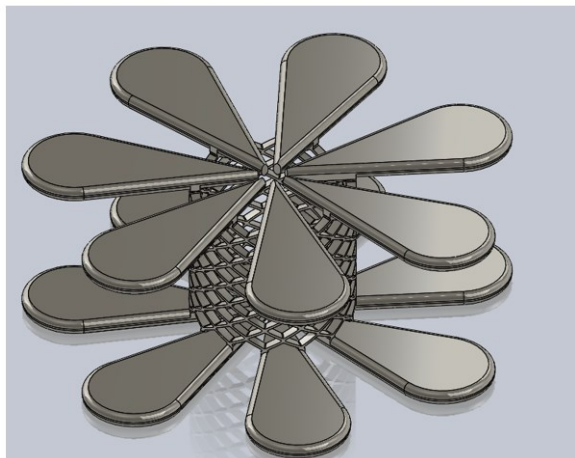


*Figure 6: First Design Iteration*

While this particular design did not envision all of the requirements such as the inclusion of the short and long overhangs, it did include the waist inspired from a stent design. There were a number of challenges with this design which caused this particular design to be discarded and further modified. The first potential problem was printability since a standard single nozzle FDM printer would be unable to produce this shape without the use of supports. The use of supports may prove to be challenging in the crevices of the waist and potentially resulted in quality issues. The main concern however was that the contact area connecting the waist with the overhangs was very small and the overhangs would have been easily detached from the waist, effectively rendering it useless. Hence, this device was unable to fulfil any design benchmarks set out in the beginning. The second iteration improved on the existing design and addressed the issue of the weak overhangs by the addition of a solid ring of material surrounding the contact area connecting the waist and the overhangs. The CAD model and 3D printed sample for this particular design iteration can be seen in Figure 7 and 8 respectively.

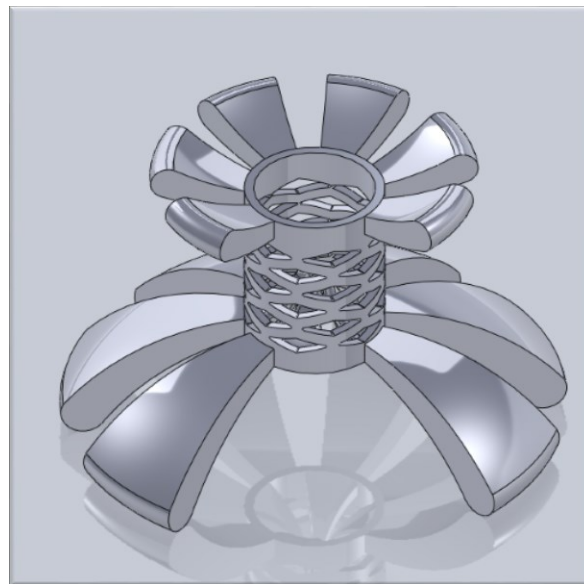


*Figure 7: CAD model for second design iteration*

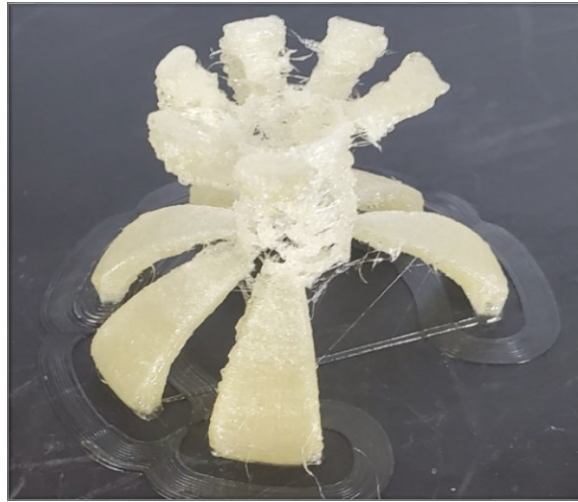


*Figure 8: 3D printed sample for second design iteration*

While this design improved on the concerns of the first iteration, it was discarded due to the curved nature of the overhangs which resulted in poor surface finish and severely affected print repeatability. This issue was quickly addressed, and the design updated to the third iteration which can be seen in Figure 9 and 10, which show the CAD model and print sample, respectively.

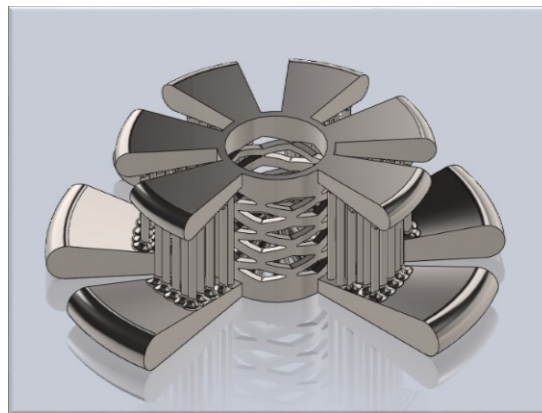


*Figure 9: CAD model for third iteration*

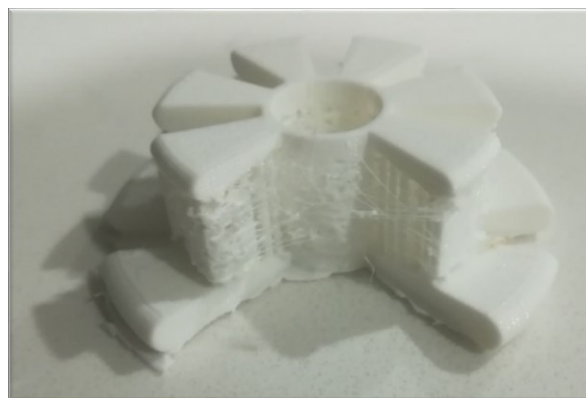


*Figure 10: 3D printed sample for third design iteration*

The main issue that was addressed in this particular iteration was the curvature of the overhangs which were kept horizontal in an attempt to improve the poor surface finish experienced by the previous design iteration. This was done by manually adding supports to the design ensuring the optimal thickness that would provide support as well considering ease of removal. An important observation that can be seen in Figure 7 through 10 is a gap between overhangs which was intentionally added to allow the spermatic cord, which ranges from 11 to 26 mm in diameter, to pass without creating any obstruction [54]. It is important to note that this design effort is not meant to yield a universal fit but in fact provide a single proof of concept within acceptable sizes ranges. While the issue of the poor surface finish was addressed with this design upgrade, this design still did not meet the design requirements and was not ready for fabrication. The overhangs were large and bulky and caused major problems for shape memory programming and recovery. An attempt made to program this design into the pre-activation shape can be seen in Figure 11.



*Figure 11: Shape memory programming of third design iteration*

As observed in Figure 11, the pre-programmed shape has poor quality, and the waist is quite damaged after programming. This design iteration cleared the printability benchmark but was

unable to clear any other benchmark. Due to the physical removal of the supports by the use of pliers, the inner sides of the overhangs had a rough surface finish which in turn resulted in low repeatability of fabrication. As seen in Figure 11, the functional requirement was also not achieved since the device was damaged during the process of shape memory programming. A common issue faced by all three design iterations was the design complexity, which caused considerably poor surface finish of the waist. Not only was the intricate design very difficult to print using the smart material, but it was also unable to change diameter from the pre-activation to the post-activation waist dimensions as intended. This was mainly due to the addition of solid material around the contact area connecting the overhangs and the waist and its effect be visualised in Figure 12 where the one of the waist endcaps was isolated and inspected.



*Figure 12: Waist endcap deformation*

Upon attempting to program any design from the first three iterations, the common problem faced was the ineffectiveness of the waist to alter its diameter. The reason for its repeated failure to achieve this was the endcap which restricted the compression of the circular ring of material connecting the overhangs. When compressed, the structure was unable to collapse on itself and

reduce in diameter. A successful reduction in diameter from 15 mm (of the waist) to 10 mm as desired by the research objective would require the circumference of this endcap to change by  $5\pi$ , which was simply not possible with the current design. While the only way forward was to modify the design of the waist, there were two potential options; the first being to further complicate the design to attempt to fix this issue, or second, modify the design as a whole and simplify it altogether addressing all of the issues simultaneously. As a result, the option to redesign the waist was considered and implemented while addressing the issue of the large and bulky overhangs as well. The fourth iteration of the design proved to be a huge step to achieve the desired design benchmarks and the CAD model and printed sample can be seen in Figure 13 and 14 respectively.

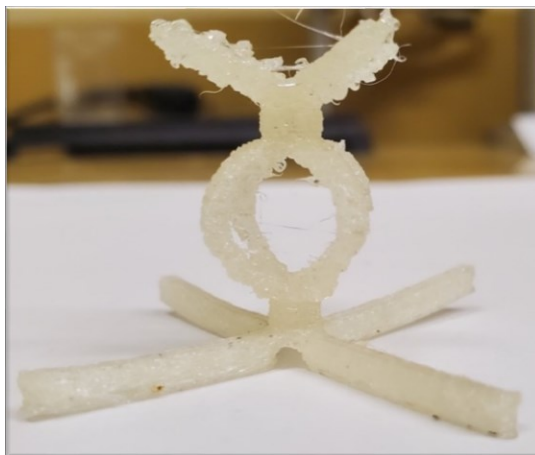


*Figure 13: CAD model for fourth iteration*



*Figure 14: 3D printed sample for fourth design iteration*

This particular design iteration was successfully able to complete the functional requirement without damaging the structure of the smart plug. This design also resolved the issue of the overhangs being bulky and large while the use of four equally spaced overhangs allowed for the smart plug to become symmetric which would be very useful for navigating the plug while in the desired location simultaneously allowing the cavity in between any two overhangs to provide the required space for the spermatic cord.

An attempt to program this design into the pre-activation shape can be seen below in Figure 15, which also shows a typical sharpie pen for comparison.

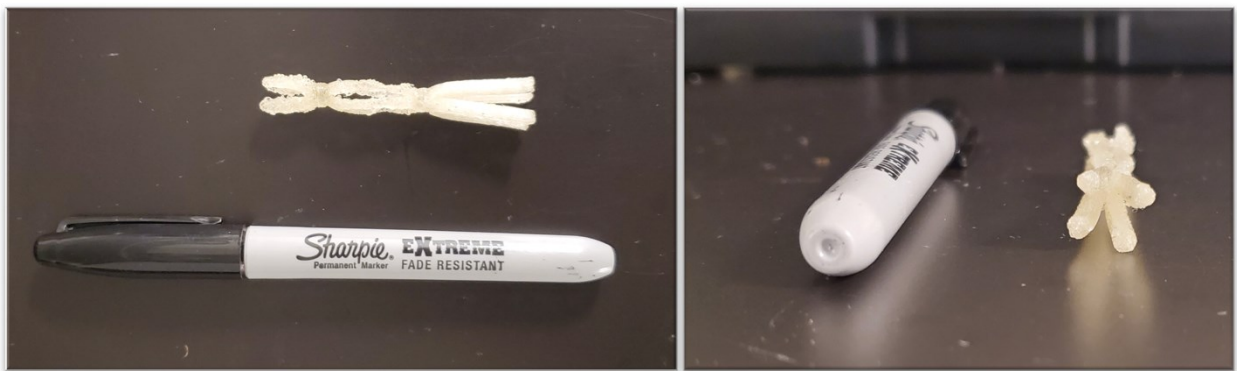


*Figure 15: Programming attempt for a 3D printed sample of the fourth design iteration*

While this programming attempt proved that this particular design iteration was able to achieve the functional requirement, there were still a few concerns that needed to be addressed such as printability and repeatability of fabrication. Both these benchmarks were not met as the current design displayed poor surface finish as well as warping in the overhangs that were in contact with the print bed as can be seen in Figure 16.

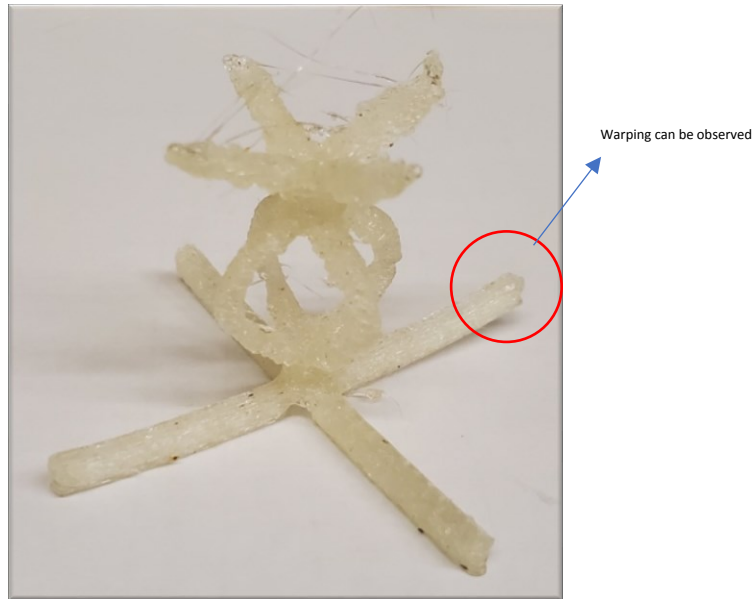


*Figure 16: Common defects in 3D printed sample of fourth design iteration*

Warping was observed to be a repeating problem observed in all of the printed samples and were attributed to the circular shape of the overhangs which caused inadequate adhesion and subsequently uneven heat transfer between the print bed and the material which caused warping. While this was quickly addressed in the next iteration by modifying the shape, there was a more inherent problem that was faced throughout the design iterations till now. The surface finish produced by a standard single nozzle FDM printer, to produce such aggressive angles, would be insufficient regardless of the print parameters. Therefore, the fabrication technique needed to account for the inclusion of supports, which were critical to achieve an acceptable surface finish. However, this alone was not adequate since the supports that were to be added must also not contribute to poor surface finish as was observed in the third design iteration. To address this concern, the use of a dual nozzle FDM printer was employed. This would allow the fabrication of the smart plug using two materials with the first primary material being the shape memory polymer and the second being a water-soluble support which would not require physical removal and therefore not contribute to poor surface finish. This breakthrough resulted in the development of

the final design iteration for which the CAD model with and without supports can be seen in Figure 17 and 18 respectively.

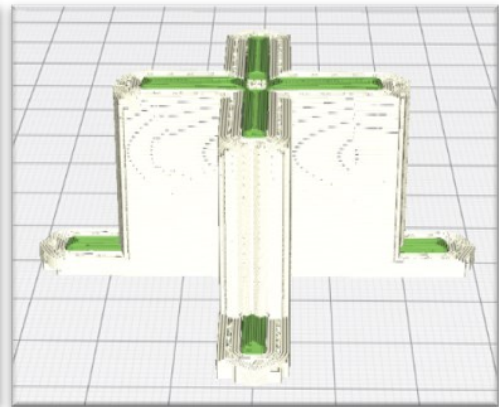


Figure 17: CAD Model of final design iteration with supports

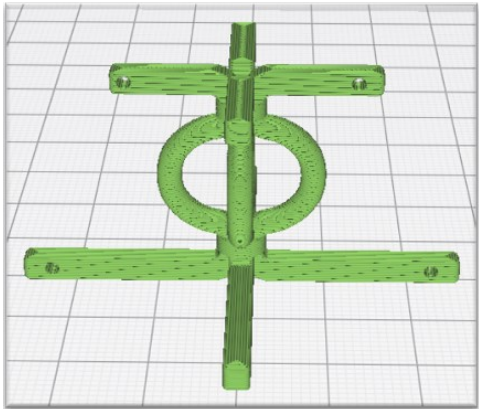


Figure 18: CAD Model of final design iteration without supports

A side-by-side comparison of a printed sample this particular design iteration with the previous iteration can be seen in Figure 19.



Figure 19: Comparison of 3D printed sample between final design iteration with fourth design iteration

It can clearly be observed that the upgraded design shows no sign of warping as compared to its previous counterpart. Another important observation was the improved overall surface finish of both the top and bottom overhangs that can be seen in the sample of the final design iteration. After further optimisation of print parameters, the samples printed yielded significantly higher overall quality as can be seen in Figure 20.

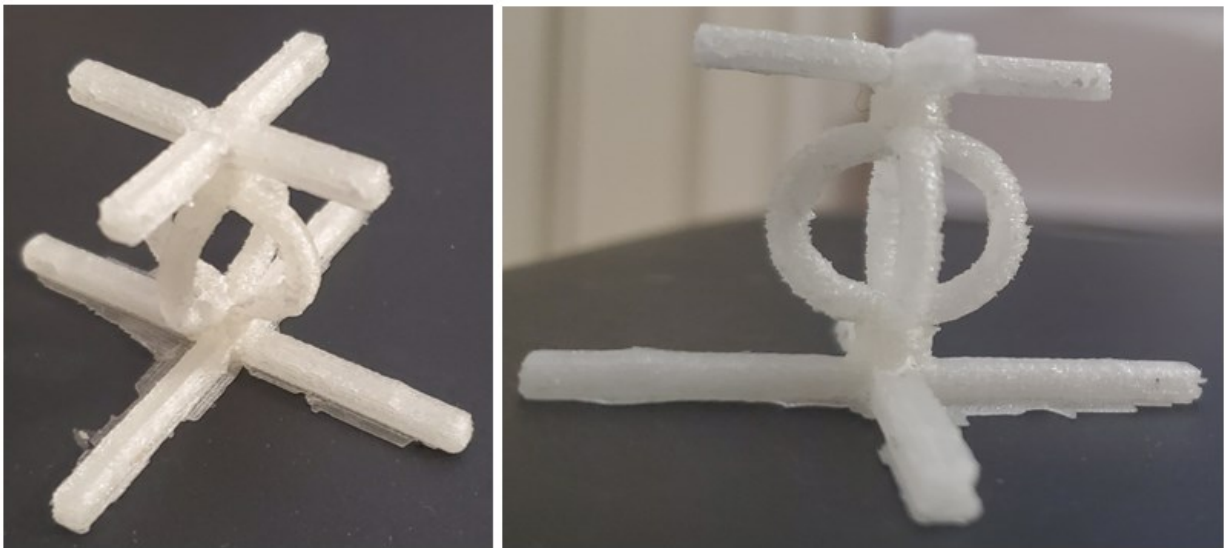


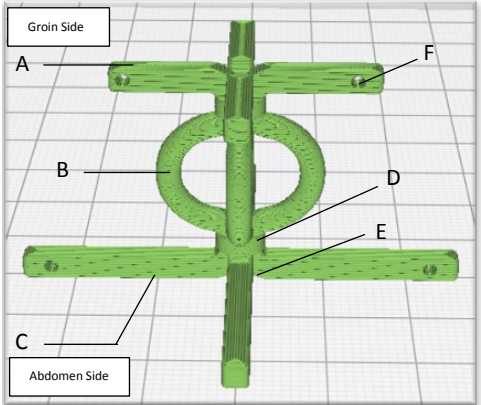
*Figure 20: Print results of final design iteration using optimised print parameters*

Comparing this particular design iterations against the design benchmarks produced promising results. Since the final design iteration was fundamentally similar to the fourth design iteration, the functional requirement was effortlessly met. The design, too, was simple unlike design iteration one through three. This particular design iteration also displayed excellent printability and repeatability in terms of fabrication being the first design iteration that successfully met all of the key benchmarks.

The short overhangs in post-activation shape had a span of 30 mm and the long overhangs had a span of 50 mm. The angle between the overhangs was 90° and was set intentionally to allow for

the spermatic cord to pass. It is imperative to note that this particular smart plug is not a universal fit and may need to be scaled or improvised to accommodate different patients. The waist of the smart plug is able to expand to a span of 20 mm with the height of the plug from long to short overhang being 27 mm. These key dimensions and design features are summarized below in Table 1.

Table 1: Summary of key design features for smart plug

	Feature	Description
 <p>The image shows a 3D CAD model of a green smart plug. It has a central vertical shaft with a circular ring in the middle. Two horizontal bars extend from the shaft, one above and one below the ring. The top bar is shorter than the bottom bar. Small circular holes are located at the corners of both horizontal bars. Labels A through F point to specific features: A points to the top bar, B to the ring, C to the bottom bar, D to the base of the ring, E to the angle between the bars, and F to the holes. A 'Groin Side' label is at the top left and an 'Abdomen Side' label is at the bottom left.</p>	A	The short overhangs span is 30 mm in diameter and is smaller due to limited space in the groin side of the body, and will assist the device in gripping in position at the site of the hernia
	B	The waist is able to expand to 20 mm (measured from the centre) and will grip the abdomen wall from the site of the cavity
	C	The long overhangs span is 50 mm in diameter and is larger due to abundance of space in the abdomen side of the body and will assist the device in gripping in position at the site of the hernia. The longer length will result in a better grip
	D	This feature assists in printability by providing a base for the waist to be printed on. The total height of the waist is 27 mm
	E	The angle between overhangs is kept at 90° and prevents obstruction of the spermatic chord that may be in vicinity of the hernia repair site
	F	Holes at the corners of the overhangs allow surgeons to attach a mesh to the device rather than the abdominal wall which will improve grip offered by the device.

The next phase of this study will discuss the fabrication phase of the research discussing the detailed approach and parameters that were employed.

### 3.2 Fabrication Phase

While the fabrication phase was closely linked to the design phase and was somewhat conducted simultaneously, it was only after the achievement of the final design that fabrication process was finalised and further optimized. During design iteration one through four, the fabrication was done using the Ultimaker 2, which was a single nozzle FDM printer. The final iteration, as discussed in the design phase, needed supports to successfully fabricate it due to which the printer used to fabricate the sample was the Ultimaker 3 (UM3), which is a dual nozzle FDM printer. The second nozzle would allow the use of secondary water-soluble supports which would stabilise the structure of the print sample as well as ensure the quality of the print sample. Printing the final design iteration with a single nozzle FDM printer was simply not possible.

Since there were two materials required to fabricate the final design, the requirement for the primary material was to have shape memory capabilities, and for the secondary, was to ensure that it could be dissolved in water. The primary material is shown as green, and the secondary material is shown as white in Figure 17.

Based on the requirement of shape memory capabilities, as well as the increased focus on the use of polymers in the development of hernia meshes, found in literature, the primary material was chosen to be thermoplastic polyurethane shape memory polymer (MM4520). The glass transition temperature ( $T_g$ ) of MM4520 used in this study was prescribed to be 45°C by the manufacturer (SMP Technologies, Tokyo, Japan). It is important to note that since the ambient condition of the smart plug was moist, a drop in  $T_g$  was expected as per the work of Irina et al., which would result in a lower  $T_g$  than 45°C [55]. The activation temperature that was required for successful deployment of the smart plug was ideally in the vicinity of human body temperature which is 37°C. This key feature would allow the smart plug to activate and instantly begin deploying upon

insertion to the hernia site. The integration of SMP particles to produce a novel shape memory surgical mesh by Zimkowski et al. is a notable achievement in the use of smart materials in hernia repair applications. Zimkowski et al. used a photo-polymerizable resin based on tert-butyl acrylate (tBA), n-butyl acrylate (nBA) and poly(ethylene glycol) dimethacrylate (PEGDMA) to develop their prototype. Their work showed that the mechanical properties, glass transition temperature ( $T_g$ ) as well as the SMP hernia mesh unrolling time was directly dependent on the network composition of the polymer. While Zimkowski et al. developed four formulas with each formula having a different  $T_g$  ranging from 57 °C to 44 °C, they concluded that the formula with the  $T_g$  of 44°C was a better candidate due to the reduced difference between the  $T_g$  and the average abdominal temperature of 37.5 °C [51]. As stated in Chapter 2, the integration of SMP with hernia repair meshes is not abundant in the literature. Due to this, the utilization and application of SMPs to develop other SMP based biomedical devices was then studied to determine a suitable candidate that could be used to fabricate the device proposed in this study. Another notable work was that done by Kim et al. who created filaments from polyurethane based SMPs (MM5520) pellets to develop 3D printed shape transformable bifurcated stents. Kim et al. attempted to improve the success rate of stent insertion procedures by developing a novel design incorporating kirigami structures which in turn removed the amount of hinderance that is faced by conventional stents and yielded promising results. The part of their study relevant to our work was the use of MM5520, which has a  $T_g$  of 55°C, and is a polyurethane based SMP. While discussing the limitations of their work, they noted that despite the potential advantages shown by their proposed design, the activation temperature which triggers the shape change from the temporary to permanent shape was too high for clinical use [56]. This added to the observation seen in the work of Zimkowski et al. and further narrowed the requirement of  $T_g$  of this study. Aside from the aspect of temperature,

the work of Kim et al. was successful in displaying the functionality of their prototype and proof of concept. Their work further directed this study to research the use of polyurethane based SMPs with a  $T_g$  being in the vicinity of 37.5°C and 44°C as deduced by reviewing the work of Zimkowski et al. The work of Chen et al. on reinforcing SMP based cardiovascular stents with cellulose nanocrystals displayed improved shape memory characteristics paving the path of MM4520 being used as a potential alternative to existing alternatives. Similar to the work of Kim et al., Yu et al. also created filaments from polyurethane based SMP pellets, which were then used to 3D print cardiovascular stents [52]. Yu et al. reported a drop in  $T_g$  (5°C) upon addition of cellulose nanocrystals, from the prescribed 45°C, and conducted their shape memory characterization at 40°C which coincides with the range provided by Zimkowski et al. The work of Yu et al. proved to be an excellent instance of the use of 3D printed SMP based polyurethane to develop low cost and effective biomedical devices, providing further confidence in the use of polyurethane based SMPs as a potential candidate for the device proposed in this study.

While the work of Zimkowski et al. helped narrow the search of a suitable material by providing a suitable range for  $T_g$  being in the vicinity of 37.5°C and 44°C, the work of Kim et al. noted that the use of materials with temperatures of  $T_g$  near the vicinity of 55°C, as done by them, was too high for clinical use. Their work also suggested that the use of polyurethane based SMPs could prove to be an excellent contender in the search for a suitable material. The work of Yu et al. further solidified the case of using polyurethane based SMPs as an ideal candidate and used MM4520 in their own work yielding promising results. In light of the information available, MM4520, a polyurethane based SMP with a  $T_g$  of 45°C seemed to be a strong contender for the smart plug proposed in this study.

The MM4520 was purchased from SMP Technologies, Tokyo, Japan, in the form of pellets and needed to be converted into filament from in order to be fed into the UM3. In order to process the pellets to filaments, they were initially dried for 12 hours in a vacuum oven (Lindberg/Blue M from Thermo Fisher Scientific Inc.), as shown in Figure 21, at 80°C similar to the technique presented in [44], to remove and prevent the ingress of moisture in the material which could potentially form voids in the filament if not done [57]. Once the pellets were dried, they were processed into filaments by polymer melt-extrusion using a 3 mm circular cross section die using a Brabender™ single screw extruder (Figure 22) attached to a drive system (Figure 23) to pull and wind the filament similar to [55].



Figure 21: Vacuum Oven - Lindberg/Blue M from Thermo Fisher Scientific Inc.



Figure 22: Brabender™ single screw extruder



Figure 23: Drive system to wind filament

The extruder heating zones, summarized in Table 2, were set to 170°C, 180°C, 190°C and 195°C for the four heating zones of the extruder, ordered from feeder to the nozzle of the extruder and were adapted from Villacres et al [57]. The extrusion rate and pulling speeds were kept constant at 15 rpm [55]. Once the filament was extruded, it is still exposed to the atmospheric humidity and is able to absorb moisture, for this reason the excess moisture was removed by drying the filaments in a vacuum oven (Lindberg/Blue M from Thermo Fisher Scientific Inc.) for 12 hours and sealed in a vacuum bag, to prevent moisture ingress, until printing was required.

*Table 2: Summary of Extrusion Heating Zone Temperatures for Extruder*

Heating Zone	1 (Feeder)	2	3	4 (Nozzle)
Temperature (°C)	170	180	190	195

The secondary material was chosen to be polyvinyl alcohol (PVA), as per the endorsements of Ultimaker which supported the use of PVA with their UM3 with benefits such as non-toxicity, reliable adhesion to a number of commonly used filaments for 3D printing, complete biodegradability excellent thermal stability and finally complete water solubility. For these reasons, PVA was purchased directly from Ultimaker (2.85 mm) to print supports while printing the final design iteration. Once the material selection was finalised, the printing parameters were then optimised and are summarised in Table 3.

Table 3: Summary of printing parameters

Printing Parameter	Value	Unit
Layer Height	0.2	mm
Nozzle Speed	10	mm/sec
Nozzle Temperature (MM4520)	220	°C
Nozzle Temperature (PVA)	220	°C
Print Bed Temperature (PVA)	70	°C
Infill	100	%
Support Layer Count	3	-
Primary Nozzle Size	0.4 (BB)	mm
Secondary Nozzle Size	0.4 (BB)	mm

The considerations summarised in Table 3 are based off repeated efforts to optimise these printing parameters against surface quality, print integrity and overall printing success as per the design benchmarks set out in the fabrication phase. Printing an individual sample with supports required approximately four hours to print and, in an effort, to increase efficiency and to reduce potential variations between printed samples, a batch production approach was considered where a set of five samples were produced at the same time. All of the samples in the batch, were printed simultaneously, since the UM3 did not support the fabrication of one sample at a time with the use of dual nozzle at the time this study was being conducted. The batch printing took approximately 26 hours to complete and generally resulted in lower number of failures as compared to the single print approach, therefore allowing for more available samples for the characterization phase of this study.

### 3.3 Characterisation Phase

The characterisation phase of this study was further sub-divided into two main sections with the first one being the mechanical characterisation which considered the endurance and integrity of the plug, and the second being the shape memory characterisation which considered the deployment speed and activation properties. The characterization phase was conducted in efforts to validate the research objective by comparing the results of this phase with those available in the literature of commercial products.

#### 3.3.1 Mechanical Characterisation

The mechanical characterisation was performed in two steps with the first being a single compression test and the second being cyclic compression testing. To better understand the justification behind conducting these tests, the loading conditions of conventional meshes must be understood along with the general stress loading in the human body in the location of the inguinal hernia.

As stated in the Chapter 2, the cause of a hernia is the weakening or breach of a particular tissue wall, making it the primary obstacle to overcome in order to attempt to fix it. In the case of this study, for the inguinal hernia, that particular tissue is the abdominal wall which is a complex composite structure composed of multiple varying layers depending upon the anatomical location. The primary purpose of the abdominal wall is to provide a mechanical barrier therefore protecting tightly packed internal organs, to support the intra-abdominal pressures (IAPs) present in the abdominal cavity as well as facilitating the natural motion of the human torso [27]. A schematic of an inguinal hernia is shown in Figure 24.

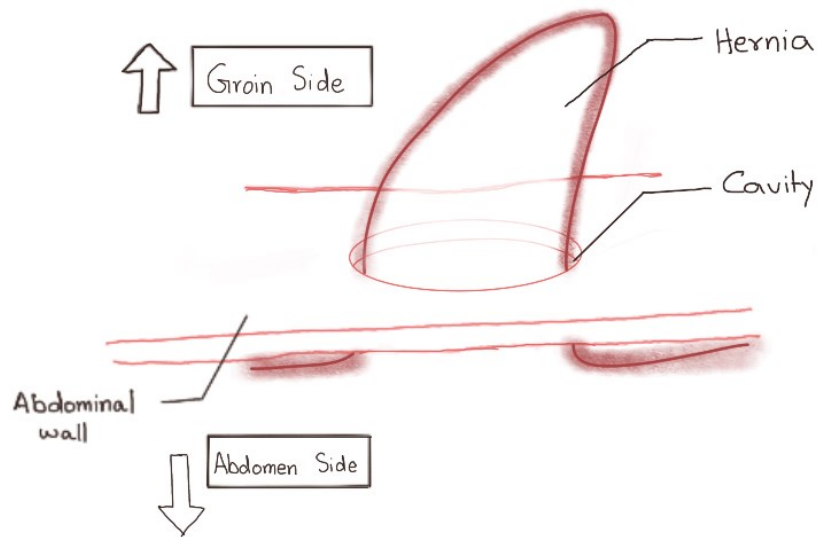


Figure 24: Schematic of Inguinal Hernia

Since an inguinal hernia impairs the mechanical function of the abdominal wall, it is critical to understand the mechanical properties of the healthy abdominal wall. The work of Klinge et al. determined that, based on the law of Laplace and maximum IAP, a mesh with a tensile strength of 16 N/cm would be sufficient for the use of hernia repair [58][59]. While this is believed to be the physiological strength of the human abdominal wall, most commercial meshes are capable of withstanding significantly higher tensile forces. Since the organs inside the abdominal cavity are held in place by the abdominal wall, it experiences a constant state of tension. Any meshes that are attached to it (Figure 25), also experience similar tensile forces, and for the case of a hernia, must be able to withstand these tensile forces.

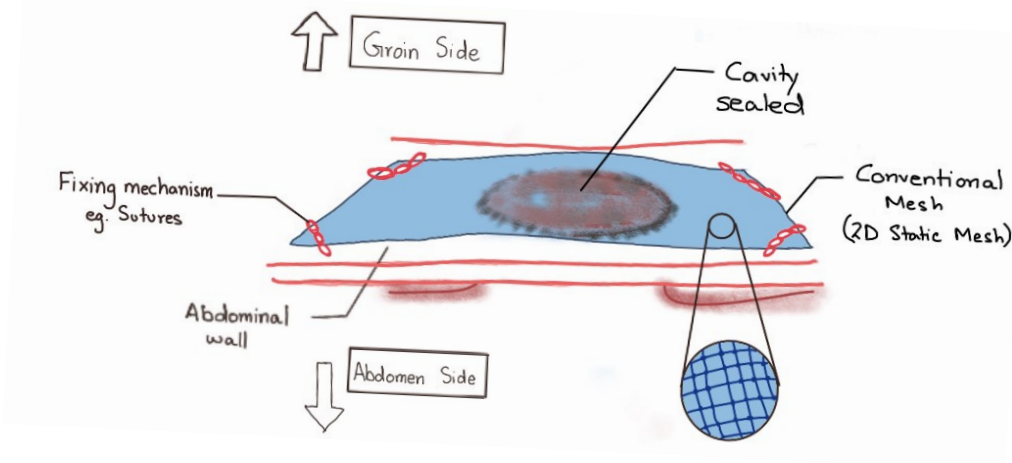


Figure 25: Schematic of conventional mesh attached to hernia site

The intra-abdominal pressure is reported to be 170 mmHg resulting in meshes being used to treat hernia repairs required to withstand at least 180 mmHg which is equivalent to 32 N/cm [59]. Owing to the difference in application of our smart plug, the force loading will be quite different from conventional meshes. Considering the weight of the contents of the abdominal cavity, the smart plug will be in a constant state of compression and must be able to withstand at least 180 mmHg or approximately 24 KPa. Due to the difference of application as well as loading from traditional meshes, a direct comparison might not be the best approach. In light of the argument presented, the first test to characterise the mechanical properties was performed by conducting a single compression test to determine the stiffness and maximum force of the smart plug before compaction, and then compared against the pressure values of the abdominal cavity as well as a few commercial alternatives. The second test conducted involved performing a cyclic compression test to study the effects of repeated and cyclic loading on the smart plug.

Both tests mentioned above were conducted using a Bose ElectroForce 3200 Series 3 test instrument which is equipped with a 450 N load cell inside a temperature chamber and can be seen in Figure 26. The temperature chamber allows us to set and maintain a certain temperature while conducting tests which is crucial for this study since all the characterisation tests conducted on the smart plug is at the normal resting human body temperature of 37°C. Once the samples were printed in a batch, they were soaked in tap water for a week which would dissolve the supports as well as allow the intake of water to simulate the moist internal environment of the human body. Upon soaking, the respective tests were conducted in the Bose machine and data was recorded and analysed.



*Figure 26: Bose ElectroForce 3200 Series 3 test instrument*

A comparison of the sample before compression compared to a fully compressed sample experiencing elastic deformation can be seen in Figure 27 and 28, respectively.



*Figure 27: Sample before compression*



*Figure 28: Sample after compression*

The single compression test was conducted by keeping the bottom plunger stationary, which was attached to the 450 N load cell with a resolution of 10% and moving the top plunger at a speed of 1 mm/sec by a total displacement of 12 mm followed by complete retraction. The temperature was kept constant at 37°C, and the force exerted by the sample was recorded with respect to displacement.

The cyclic compression test was conducted under similar test conditions with the only change being the displacement of 11 mm and instead of a single test being conducted, a total of 10 cycles were performed, respective force and displacement values recorded and then analysed, as similarly done by Roman et al [60].

### 3.3.2 Shape Memory Characterization

The shape memory characteristics mainly involved the study of the shape recovery ratio and the shape recovery speed. It is important to note that since the structure is divided into three main

components; waist, short overhangs, and long overhangs, as shown earlier in Figure 5, the shape memory characteristics for each of these components were measured and analysed separately.

The sample was initially intended to be preheated to 50°C ( $T_g+5^\circ\text{C}$ ) to program the pre-activation shape as done by Irina et al.[55], however due to soaking of the sample in water for a week to dissolve the supports and replicate the abdominal environment, the sample was able to be programmed at a much lower temperature while displaying significant flexibility even at room temperature. This phenomenon was attributed to the lowering of  $T_g$  due to the absorption of water and is explained in the work of Irina et al [55]. In light of this, the oven (Lindberg/Blue M from Thermo Fisher Scientific Inc.) was preheated to 45 °C, and the sample was placed in the oven for a duration on 15 minutes and an initial image was taken as reference for that particular sample. To program the pre-activation shape onto the sample, the sample was pushed into a brass tube of internal diameter of 12.5 mm and placed inside an ice bath. The oven was allowed to cool and was then reheated to 37 °C while the enclosed sample soaked in the ice bath. The next step proved to be time sensitive and required significant agility, since upon exposing the sample to room temperature air caused activation to initiate, the remaining experimental setup needed to be setup beforehand. The brass tube was removed underwater inside the ice bath to ensure that the sample does not activate and then immediately placed inside the oven. The activation of the sample was recorded using a Basler acA3800-10gm GigE camera. The camera was calibrated to take pictures of the deploying smart plug at a frequency of 4 Hz. A regular paper tape was also kept in the shot and was pre-measured and placed such that the centre of the tape would overlap with the suspended smart plug in an effort to negate any errors due to depth of field. An image sample of the pre-activation and post-activation capture by the camera can be seen in Figure 29 and 30 respectively.



*Figure 29: Pre-activation Image recording activation*



*Figure 30: Post-activation Image recording activation*

These series of images were collected and then further processed in ImageJ to measure the angle of deployment of the short and long overhangs as well as the expansion of waist. To measure this information, a few points were marked as reference and were tracked and measured manually with the appropriate scale which was calibrated using the paper tape in the bottom of the image in Figure 29 and 30. The process of marking, tracking, and measuring these points were done on all of the images for a total of three samples and can be seen in Figure 31 and 32 which shows the pre-activation and post-activation shape respectively. This information was then analysed to measure the shape recovery ratio which is defined as the ratio of shape recovery for each component from pre-activation to post-activation and finally compared to the original reference taken in the start.



*Figure 31: Pre-activation image recording activation with tracking points*



*Figure 32: Post-activation image recording activation*

The recovery speed was also calculated using the above technique and is defined as the recovery of shape with respect to time while also providing us with total time required to activate completely and attain post activation shape.

## Chapter 4: Results & Discussion

The data obtained from the characterisation was analysed and then compared to known commercial alternatives found in literature to determine the results of this study as discussed in this chapter.

### 4.1 Mechanical Characterization

The results of the mechanical characterisation included the single compression test as well as cyclic compression test, based on the techniques specified in Chapter 3.

#### 4.1.1 Compression Testing

The force versus displacement graph plotted for all samples yielded similar graphs can be seen in Figure 33. The two important parameters that were generated from this particular experiment were the stiffness of the smart plug as well as the maximum force before compaction. The smart plug experiences full compaction at approximately just over 11 mm of compressive displacement and a picture of the sample before and after compression are shown in Figure 27 and 28 (Chapter 3). The full compaction region can be seen in the red shaded area in Figure 33. This region was discarded for analysis purposes since sufficient data, required to present a detailed discussion, was not collected keeping in mind equipment safety concerns. This importance of presenting this region was to show that despite compaction, the sample did not show signs of failure.

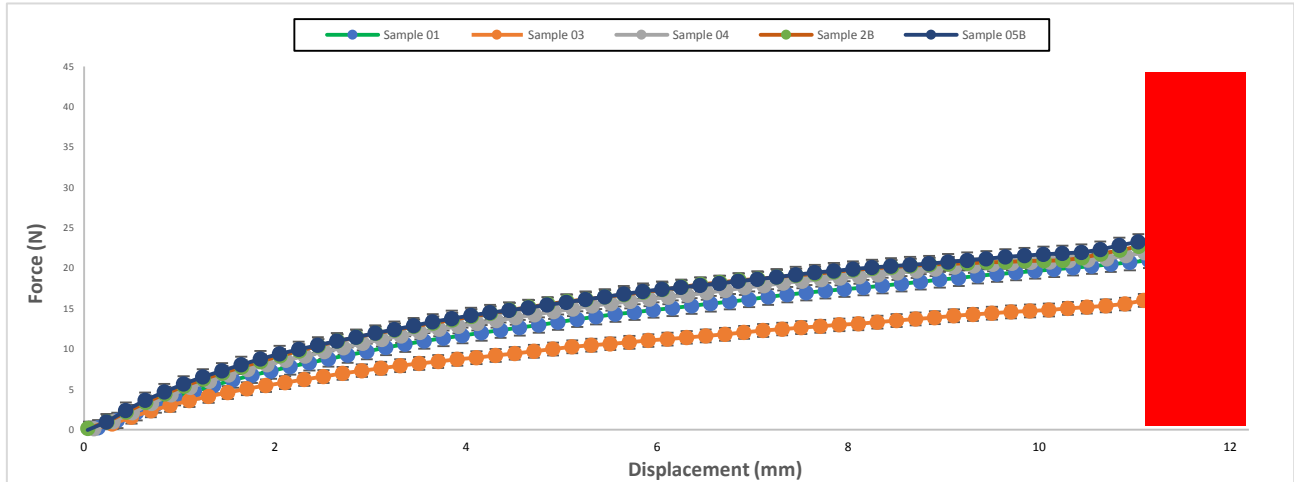


Figure 33: Force versus Displacement graph for all samples

The equipment safety concerns were due to the load cell of 450 N, attached to the Bose ElectroForce 3200 Series 3 test instrument (Figure 26). As the samples experienced full compaction, the force experienced by the plug increased exponentially with smaller increments of displacement. This could potentially damage the load cell used to measure the force or trigger the electronic safety load value causing the machine to abruptly shut off. Therefore, for all intent and purposes of this study, the region before full compaction was considered for analysis. Since the sample exhibited compaction at 11 mm, the value of maximum force therefore was taken at 11 mm of compressive displacement for all samples. The value of all five samples were recorded and averaged to generate a single value, for reporting purposes. The averaged value of maximum compressive force was then compared with averaged values of maximum tensile force found in literature, which provided the maximum tensile force for a few commercial meshes before tearing, and was found to be within range of its commercial counterparts [61]. As explained in Chapter 3, it is important to note that due to the difference in loading conditions and application of the design proposed in this study and conventional meshes a direct comparison was not possible. The stiffness of the smart plug was determined by calculating the slope of individual plots shown in Figure 34 with a similar approach to analyse and discuss its validity as that of the maximum force parameter.

The method used to calculate maximum force as well as stiffness is presented in Figure 34 for one sample, with both these parameters isolated. The maximum force, as discussed earlier in this section, was noted to be the corresponding force at 11 mm of compression and is marked in red in Figure 34. The stiffness of the smart plug was calculated to be the slope of the graph and is marked in black with the corresponding values required to calculate the slope marked in orange as shown in Figure 34.

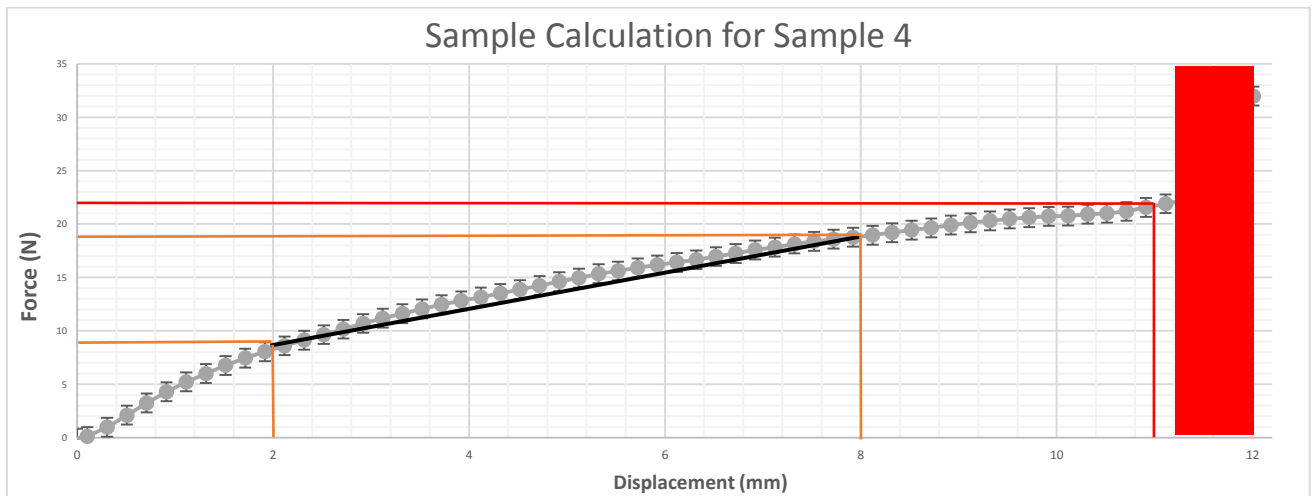


Figure 34: Model calculation for single compression test

The maximum compressive force experienced by the sample shown in Figure 34 is 22 N. The slope to calculate stiffness is measured from 2 mm to 8 mm and is calculated to be 1.667 N/mm which is equivalent to 16.67 N/cm as shown below:

$$\text{Stiffness} = \text{Slope of graph} = \frac{y_2 - y_1}{x_2 - x_1} = \frac{19 - 9}{8 - 2} = \frac{10}{6} = 1.667 \text{ N/mm}$$

Another important observation when reviewing literature was the reporting of tensile strength in units of N/cm. While this is non-intuitive and is not consistent with the definition of tensile strength, it has been reported as the maximum force with respect to clamping width as explained in Chapter 2. In order to draw a comparison between our calculated value and the available data in literature, the measured value of maximum force, reported to be 22 N was also converted to

similar units by dividing the value of maximum force by the maximum displacement (11 mm) before compaction. The sample calculation is shown below:

$$\text{Maximum Force (N/cm)} = \frac{\text{Maximum Force}}{\text{Maximum Displacement}} = \frac{22}{11} \cdot \frac{N}{mm} = 2 \text{ N/mm} = 20 \text{ N/cm}$$

Similar to this model calculation, the remaining samples were examined and the values for maximum force and stiffness were calculated, tabulated, and can be found in Table 4.

Table 4: Summary of results for single compression test

Sample No.	Maximum Force (N/cm)	Stiffness (N/mm)
1	19.1	1.75
2	20.0	1.60
3	14.5	1.25
4	20.0	1.67
5	20.1	1.61
Average	18.74	1.58

Comparing these values with the range provided in the work of Pott et al [61], for commercial meshes including Dynamesh-IPOM, Parietene, Prolene, Surgi-pro, Ultra-pro and Vicryl, provided promising results. The maximum force parameter, before failure, for these commercial products were measured to be in the range of 11.1 N/cm to 100.9 N/cm and is summarized in Table 5.

Table 5: Mechanical properties of commercial alternatives [61]

Property	Dynamesh-IPOM	Parietene	Prolene	Surgi-pro	Ultra-pro	Vicryl
Maximum Force (N/cm)	11.1	38.9	84.8	38.6	100.9	78.2
Stiffness (N/mm)	0.3	0.9	3.6	1.3	4.3	4.6

With an average maximum force measured to be 18.74 N/cm, our proposed smart plug was well within acceptable range of 11.1 N/cm to 100.9 N/cm displayed by commercial alternatives. The wide range of values of maximum force and stiffness displayed by commercial alternatives is attributed to the type of mesh being either heavy weight mesh or light weight mesh as well as difference due to material properties used to manufacture the mesh. It is also important to note that upon full compaction, the smart plug did not show any signs of failure and recovered to its post-activation shape without any major signs of plastic deformation. The value calculated in this study is therefore a very conservative value and while although is not a direct comparison to these meshes, it is able to endure similar loading conditions with ease. The stiffness parameter was reported to be in the range of 0.3 N/mm to 4.6 N/mm by Pott et al. , as shown in Table 5, and the value of our proposed design was 1.58 N/mm, as shown in Table 4, was well within the acceptable range [61]. The compression test was therefore successful in validating our results and proved that the proposed smart plug was at par with commercial alternatives in terms of the mechanical parameters discussed.

#### 4.1.2 Cyclic Compression Test

The result of the cyclic compression test also yielded positive results under similar loading conditions to that of compression test. The notable differences, as stated in Chapter 3, were that the test was conducted for 10 continuous cycles with the displacement being limited to 11 mm to avoid full compaction keeping in mind the safety concerns for the equipment. This test was conducted in similar set up, as mentioned in Section 4.1.1 of this chapter, with the Bose ElectroForce 3200 Series 3 test instrument (Figure 26) used to conduct the test and the sample loaded from no compressive displacement to compaction similar to Figure 27 and Figure 28. This process was repeated for a total of ten times for three samples, with data points plotted and shown

in Figure 35. All samples in this experiment experienced approximately 2 mm of plastic deformation under cyclic loading, with the plastic deformation between the first and tenth cycle of each sample marked in Figure 35. The average plastic deformation for all three samples was calculated to be 7.40 % of compressive strain and was a calculated by using the formula:

$$\frac{(\text{Displacement of 10th Cycle} - \text{Displacement of 1st Cycle})}{\text{Total height of sample}} = \frac{2 \text{ mm}}{27 \text{ mm}} \% = 7.40 \%$$

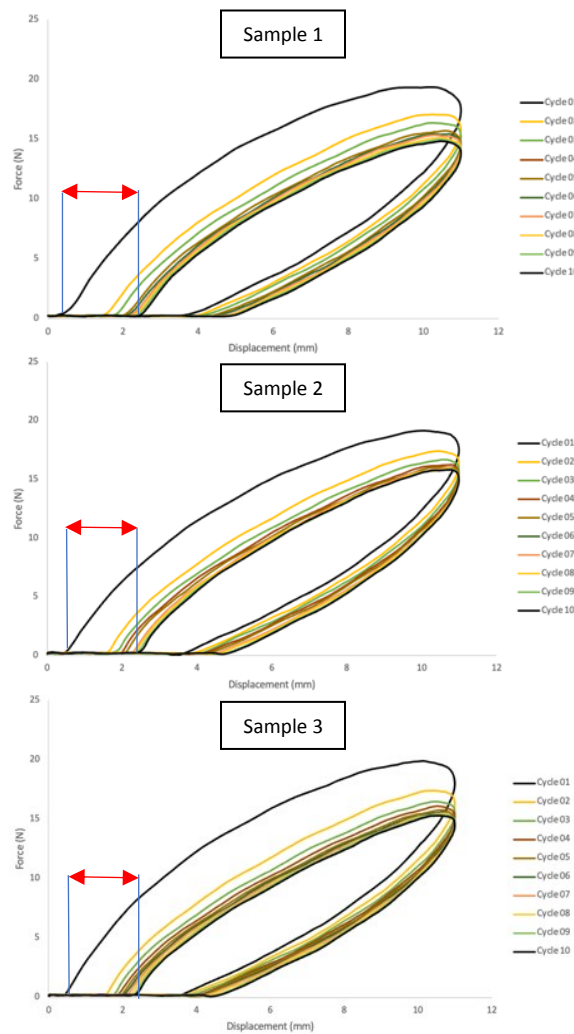


Figure 35: Plastic deformation under cyclic loading

As stated in Chapter 3, the purpose of conducting a cyclic compression test was to study the effect of cyclic loading on the deformation of the proposed design. Similar to the work of Roman et al.

[62] who conducted this test to study the effects of cyclic tensile loading on a few commercial meshes, this study conducted a similar test under cyclic compressive loading. While the work of Roman et al. was under tension and this study attempted to replicate similar results under compression, it is important to note, as stated in Chapter 3, this was done due to the difference in loading conditions that experienced by the smart plug and conventional meshes. Roman et al. studied commercial meshes including Gynemsh, Restorelle, ENDOLAP, PR4, Upy-PC and PU which displayed percentage deformation ranging from 0.58% to 8.51%. This value was calculated by measuring the deformation between the first cycle and last cycle of deformation during cyclic loading. The smart plug proposed by this study displays approximately 7.40% of permanent deformation which is within range of those available in the study by Roman et al. It also displays a similar cyclic loading pattern and may be deemed acceptable keeping in mind that this is not a direct comparison and small differences are expected.

#### 4.2 Shape Memory Characteristics

As per the techniques mentioned in Chapter 3, the shape memory characteristics were determined by investing two parameters namely, shape recovery ratio and shape recovery speed. Once the pictures of the activating sample were taken and data analysed according to the procedure in Chapter 3, a “recovery ratio vs time” graph was plotted to determine these two parameters. The recovery ratio was a normalised number determined from the ratio of the change in displacement or angle with respect to the original reference picture taken before shape memory programming. The slope of this graph was considered as the shape recovery speed while the recovery ratio value at 240 seconds after activation was considered as final shape recovery ratio. It is important to note, as stated in Chapter 3, the three main components of the smart plug, namely the shorter overhangs, longer overhangs as well as the waist, were investigated and characterised separately for three

samples. As previously mentioned in Chapter 3, the pictures for the experimental setup, pre-activation and post-activation can be seen in Figure 29 through 32.

The raw data obtained for the short and long overhangs was smoothed using a five-point moving average using MATLAB and plot accordingly and can be seen in Figure 36 and 37 respectively.

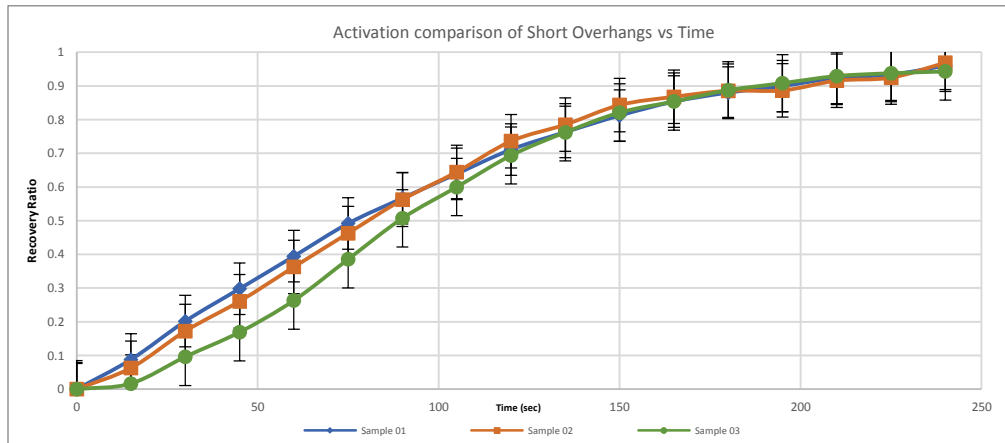


Figure 36: Activation comparison of short overhangs

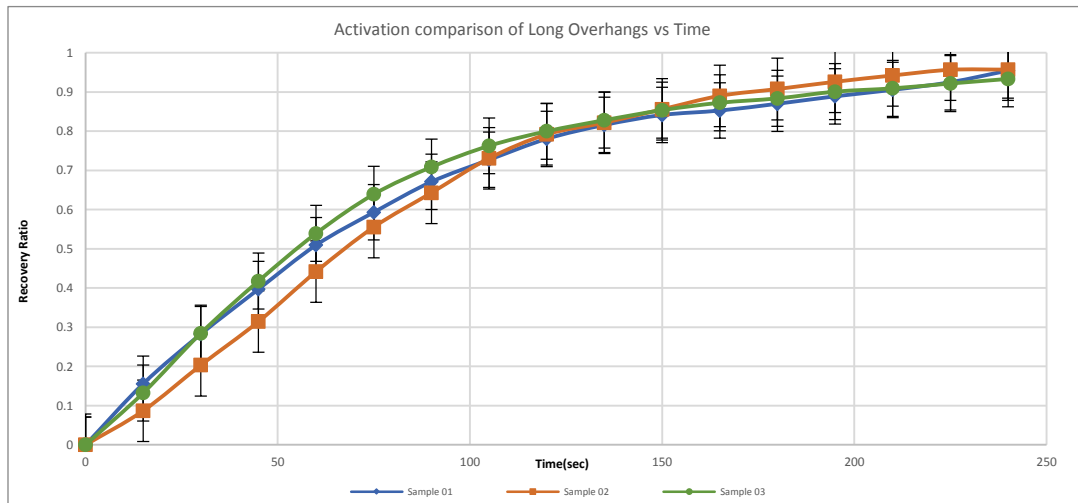


Figure 37: Activation comparison of long overhangs

With acceptable variation among samples, the deployment of the short and long overhangs experienced shape recovery of more than 90% within 240 seconds of activation. It was interesting to note that the long and short overhangs experience shape recovery at different activation speed which can be observed in Figure 38, which contains the averaged values of the three samples.

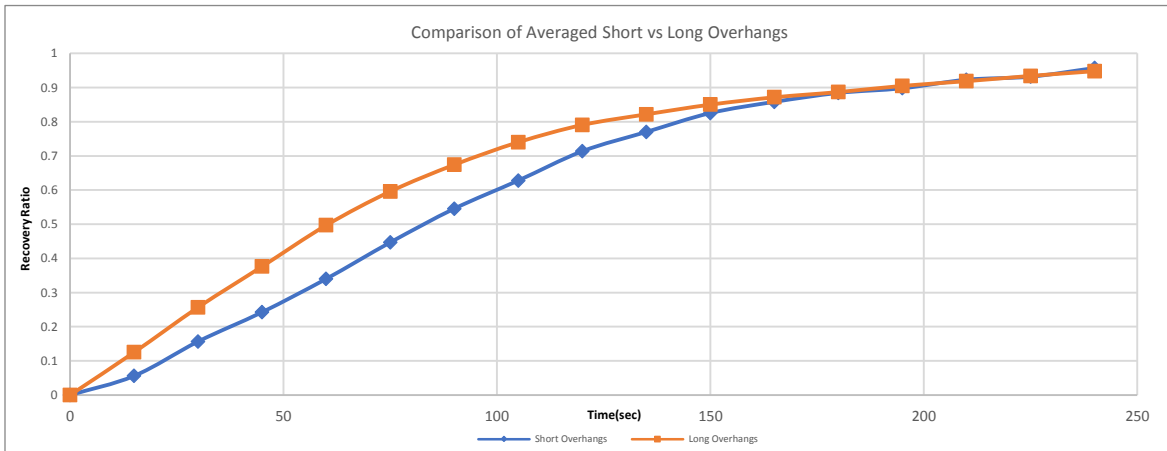


Figure 38: Recovery comparison of short vs long overhangs

As seen in Figure 38, the deployment of the long overhangs is faster in comparison to the short overhangs, with the averaged speed of activation being calculated by measuring the slope of the two graphs in Figure 38 from 0 to 100 seconds. The averaged activation speed for the short and long overhangs is calculated to be  $0.0060 \text{ sec}^{-1}$  and  $0.0073 \text{ sec}^{-1}$  respectively which is equivalent to  $0.540 \text{ %/sec}$  and  $0.657 \text{ %/sec}$ , respectively.

The raw data obtained for the waist of the smart plug was mapped using curve fitting and the data points subsequently plotted as polynomial of the third degree. With acceptable variation between samples, the activation comparison of the waist can be seen in Figure 39.

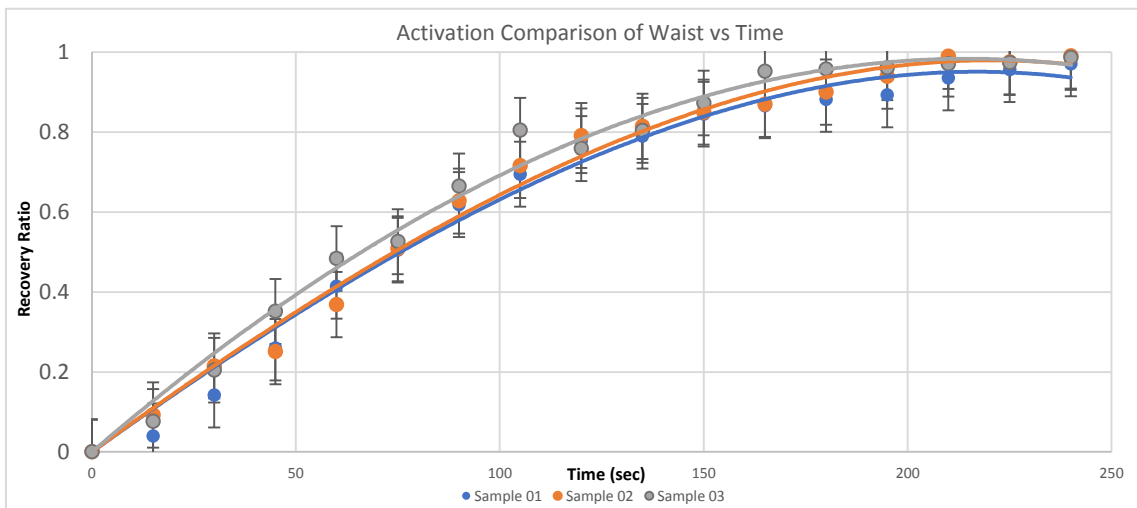


Figure 39: Activation comparison of waist

Similar to the short and long overhangs, the waist also exhibits shape recovery of greater than 90% by 240 seconds. The samples also demonstrated an average waist activation speed of  $0.0067 \text{ sec}^{-1}$  which is equivalent to  $0.0181 \text{ mm/sec}$ .

The work of Zimkowski et al. on the development of a novel SMP based hernia repair mesh, explained in Chapter 3 of this study, showed promising results with a deployment time of 31 seconds [51]. While this is a huge difference in comparison to the smart plug proposed by this study it is also important to note that the degree of assistance provided to position the mesh by Zimkowski et al. is not known. Also, the time reported by Zimkowski et al. also does not take into consideration the time taken to secure the mesh with the sutures or tacks. Since the smart plug proposed in this study is self gripping and does not require any external mechanism to secure it, the time taken to secure it in situ is also saved. It is also important to note, that once again, a direct comparison was not possible due to the difference in the nature of utilization of the device.

## Chapter 5: Conclusion and Future Works

This study was successfully able to determine a suitable conclusion for the research objective laid out in Chapter 1. The smart plug proposed by this study has the capability to be effectively and efficiently transported to the hernia repair site, using current laparoscopic technologies, keeping in mind dimensional requirements and limitations. The results of the shape memory characterisation have also shown that upon navigating to the site of the hernia repair, the smart plug can achieve maximum deployment within four minutes of activation which is not unpractical keeping in mind the complexity of current hernia repair surgeries. The results of the mechanical characterisations also demonstrated an acceptable conformity of the mechanical strength of the proposed smart plug in a variety of commercial products available. With this thesis presented, the proposed smart plug seems to be an acceptable alternative to commercial meshes and justifies further investigation into its benefits as well as limitations.

Some improvements that may be addressed in future works includes a change in manufacturing method from 3D printing to injection molding which will yield a better sample, in terms of quality and surface finish, in comparison to samples produced in this study. While this study does prove the potential functionality of the smart plug, further investigation is required to determine the performance of the smart plug in actual abdominal conditions. A mesh could also be attached to the smart plug itself to increase effectiveness of the device. Since the mesh would not be attached by sutures or tacks, this may lead to lower inflammation, scar tissue and subsequent pain experienced by the patient. The smart plug characterisations with the added mesh may need to be re-evaluated. Another important future work involves the coating of the current smart plug with a synthetic material which will minimise any inflammation caused due to foreign body rejection by the body. This will require further re-evaluation of mechanical and shape memory characteristics

to determine the smart plug performance. Simultaneously, reinforcing the smart plug with non-cytotoxic reinforcing agents such as CNC as done by Chen et al.[52] may also improve shape memory characteristics and justifies further investigation. Furthermore, it is critical to move forward with porcine models or other environments to investigate the application of the smart plug in a more realistic abdominal environment to determine the limitations of the current proposed smart plug.

While this study was able to achieve its scope of work set out in the research objectives while addressing the research questions early in the study, there were quite a few aspects of the proposed smart plug that were not investigated. This study did not investigate the biocompatibility of MM4520 for its use in manufacturing hernia repair meshes. While it is true that MM4520 has displayed acceptable biocompatibility, as described in Chapter 2, further investigation needs to be conducted in animals to determine if a human study would be possible. It is important to note as well that the purpose of this study was to develop a proof of concept and the dimensions of the smart plug may need to be adjusted on a case-by-case basis. Due to the low cost of 3D printing, this may not be an issue, however, must be mentioned. Lastly, the majority of studies that investigated the mechanical and structural properties of hernia meshes did so in situ, also providing the long-term durability of the mesh inside the body. Due to the possibility of degradation caused weakening, meshes may lose their strength over time and this aspect was also not investigated. Significant delays caused by closures due to COVID-19, that resulted in the scope and speed of this study both being severely affected, this study was unable to investigate additional properties such as shape recovery force which is also recommended as future works.

This study concludes, in light of the argument presented in this thesis, that the smart plug proposed in this thesis is at par with different commercial alternatives and justifies further investigation.

This study presents an alternative to existing conventional hernia meshes addressing its inherent flaws, improved patient care, lower cost of production as well as increased ease of surgery.

## Bibliography

- [1] J. R. Siewert, “Hiatushernie und rezidive: Ein historischer überblick und kommentar zur Arbeit von R. Pointner und F.A. Granderath,” *Chirurg*, vol. 79, no. 10. Springer, pp. 982–983, Oct. 18, 2008, doi: 10.1007/s00104-008-1583-x.
- [2] G. H. Sakorafas *et al.*, “Open tension free repair of inguinal hernias; the Lichtenstein technique,” *BMC Surg.*, vol. 1, pp. 1–3, Oct. 2001, doi: 10.1186/1471-2482-1-3.
- [3] G. Amato *et al.*, “Fixation free inguinal hernia repair with the 3D dynamic responsive prosthesis ProFlor: Features, procedural steps and long-term results,” *Int. J. Surg. Open*, vol. 21, pp. 34–43, Jan. 2019, doi: 10.1016/j.ijso.2019.10.008.
- [4] Y. W. Novitsky *et al.*, “Immunohistochemical analysis of host reaction to heavyweight-, reduced-weight-, and expanded polytetrafluoroethylene (ePTFE)-based meshes after short- and long-term intraabdominal implantations,” *Surg. Endosc. Other Interv. Tech.*, vol. 22, no. 4, pp. 1070–1076, Apr. 2008, doi: 10.1007/s00464-007-9737-3.
- [5] L.-M. Zhu, P. Schuster, and U. Klinge, “Mesh implants: An overview of crucial mesh parameters,” *World J. Gastrointest. Surg.*, vol. 7, no. 10, pp. 226–36, Oct. 2015, doi: 10.4240/wjgs.v7.i10.226.
- [6] P. K. Amid, “Classification of biomaterials and their related complications in abdominal wall hernia surgery,” *Hernia*, vol. 1, no. 1, pp. 15–21, May 1997, doi: 10.1007/bf02426382.
- [7] G. Amato *et al.*, “Enhanced angiogenesis in the 3D dynamic responsive implant for inguinal hernia repair ProFlor,” *Artif. Organs*, vol. 00, pp. 1–10, 2021, doi: 10.1111/aor.13926.
- [8] A. Kingsnorth, “Hernia: Types, Treatments, Symptoms, Causes & Prevention,” 2004. <https://my.clevelandclinic.org/health/diseases/15757-hernia> (accessed May 17, 2021).
- [9] R. Janicki and D.B. Allardyce MD FRCS, “Hernias.” Accessed: May 17, 2021. [Online]. Available: <https://gidiseasesandcomplications.com/hernia/hernia.pdf>.
- [10] O. Guillaume, A. H. Teuschl, S. Gruber-Blum, R. H. Fortelny, H. Redl, and A. Petter-Puchner, “Emerging Trends in Abdominal Wall Reinforcement: Bringing Bio-Functionality to Meshes,” *Advanced Healthcare Materials*, vol. 4, no. 12. Wiley-VCH Verlag, pp. 1763–1789, Aug. 01, 2015, doi: 10.1002/adhm.201500201.

- [11] P. Primatesta and M. J. Goldacre, "Inguinal hernia repair: Incidence of elective and emergency surgery, readmission and mortality," *Int. J. Epidemiol.*, vol. 25, no. 4, pp. 835–839, Aug. 1996, doi: 10.1093/ije/25.4.835.
- [12] C. M. P. Claus *et al.*, "Laparoscopic inguinal hernioplasty after radical prostatectomy: Is it safe? Prospective clinical trial," *Hernia*, vol. 18, no. 2, pp. 255–259, 2014, doi: 10.1007/s10029-013-1204-6.
- [13] B. Kulah *et al.*, "Presentation and outcome of incarcerated external hernias in adults," *Am. J. Surg.*, vol. 181, no. 2, pp. 101–104, Feb. 2001, doi: 10.1016/S0002-9610(00)00563-8.
- [14] "Hernia Repair Market by Product, Type & Geography | COVID-19 Impact Analysis | MarketsandMarkets," *Markets and Markets*.  
<https://www.marketsandmarkets.com/Market-Reports/hernia-mesh-devices-market-203245450.html> (accessed May 19, 2021).
- [15] K. Arslan, B. Erenoglu, E. Turan, H. Koksall, and O. Dogru, "Minimally invasive preperitoneal single-layer mesh repair versus standard Lichtenstein hernia repair for inguinal hernia: a prospective randomized trial," *Hernia*, vol. 19, no. 3, pp. 373–381, Jun. 2015, doi: 10.1007/s10029-014-1306-9.
- [16] K. A. LeBlanc and W. V. Booth, "Laparoscopic repair of incisional abdominal hernias using expanded polytetrafluoroethylene: Preliminary findings," *Surg. Laparosc. Endosc.*, vol. 3, no. 1, pp. 39–41, Feb. 1993, Accessed: May 25, 2021. [Online]. Available: <https://europepmc.org/article/med/8258069>.
- [17] D. Berger *et al.*, "Laparoscopical repair," in *Recurrent Hernia: Prevention and Treatment*, Springer Berlin Heidelberg, 2007, pp. 223–251.
- [18] A. Baktir *et al.*, "The effects of different prosthetic materials on the formation of collagen types in incisional hernia," *Hernia*, vol. 17, no. 2, pp. 249–253, Apr. 2013, doi: 10.1007/s10029-012-0979-1.
- [19] S. B. Orenstein, E. R. Saberski, D. L. Kreutzer, and Y. W. Novitsky, "Comparative analysis of histopathologic effects of synthetic meshes based on material, weight, and pore size in mice," *J. Surg. Res.*, vol. 176, no. 2, pp. 423–429, Aug. 2012, doi: 10.1016/j.jss.2011.09.031.
- [20] C. D. Klink *et al.*, "Comparison of long-term biocompatibility of PVDF and PP meshes," *J. Investig. Surg.*, vol. 24, no. 6, pp. 292–299, Oct. 2011, doi:

- 10.3109/08941939.2011.589883.
- [21] A. Coda, R. Lamberti, and S. Martorana, "Classification of prosthetics used in hernia repair based on weight and biomaterial," *Hernia*, vol. 16, no. 1. Springer, pp. 9–20, Feb. 12, 2012, doi: 10.1007/s10029-011-0868-z.
- [22] B. B. Agarwal, K. A. Agarwal, T. Sahu, and K. C. Mahajan, "Traditional polypropylene and lightweight meshes in totally extraperitoneal inguinal herniorrhaphy," *Int. J. Surg.*, vol. 8, no. 1, pp. 44–47, Jan. 2010, doi: 10.1016/j.ijisu.2009.08.014.
- [23] J. Conze *et al.*, "Randomized clinical trial comparing lightweight composite mesh with polyester or polypropylene mesh for incisional hernia repair," *Br. J. Surg.*, vol. 92, no. 12, pp. 1488–1493, Dec. 2005, doi: 10.1002/bjs.5208.
- [24] M. A. T. Muftuoglu *et al.*, "The comparison of heavyweight mesh and lightweight mesh in an incisional animal model," *Hernia*, vol. 14, no. 4, pp. 397–400, Aug. 2010, doi: 10.1007/s10029-010-0647-2.
- [25] W. S. Cobb *et al.*, "Textile Analysis of Heavy Weight, Mid-Weight, and Light Weight Polypropylene Mesh in a Porcine Ventral Hernia Model," *J. Surg. Res.*, vol. 136, no. 1, pp. 1–7, Nov. 2006, doi: 10.1016/j.jss.2006.05.022.
- [26] A. International and files indexed by mero, "D 123 – 03."
- [27] C. R. Deeken and S. P. Lake, "Mechanical properties of the abdominal wall and biomaterials utilized for hernia repair," *Journal of the Mechanical Behavior of Biomedical Materials*, vol. 74. Elsevier Ltd, pp. 411–427, Oct. 01, 2017, doi: 10.1016/j.jmbbm.2017.05.008.
- [28] A. Rastegarpour, M. Cheung, M. Vardhan, M. M. Ibrahim, C. E. Butler, and H. Levinson, "Surgical mesh for ventral incisional hernia repairs: Understanding mesh design," *Plast. Surg.*, vol. 24, no. 1, p. 41, Mar. 2016, Accessed: Jul. 23, 2021. [Online]. Available: /pmc/articles/PMC4806756/.
- [29] A. Costa *et al.*, "Biological scaffolds for abdominal wall repair: Future in clinical application?," *Materials*, vol. 12, no. 15. MDPI AG, Aug. 01, 2019, doi: 10.3390/ma12152375.
- [30] "Fixation-free inguinal hernia repair using a dynamic self-retaining implant - PubMed." <https://pubmed.ncbi.nlm.nih.gov/23065807/> (accessed May 27, 2021).
- [31] P. K. Amid, A. G. Shulman, I. L. Lichtenstein, and M. Hakakha, "Biomaterialien in der

- hernienchirurgie und ihre anwendung,” *Langenbecks Arch. Chir.*, vol. 379, no. 3, pp. 168–171, 1994, doi: 10.1007/BF00680113.
- [32] B. Klosterhalfen, K. Junge, and U. Klinge, “The lightweight and large porous mesh concept for hernia repair,” *Expert Review of Medical Devices*, vol. 2, no. 1. Future Drugs Ltd, pp. 103–117, 2005, doi: 10.1586/17434440.2.1.103.
- [33] “Scopus - Document details - Efficacy of 3D max mesh versus common mesh for laparoscopic inguinal hernia repair.” [https://www-scopus-com.login.ezproxy.library.ualberta.ca/record/display.uri?eid=2-s2.0-85097081679&origin=resultslist&sort=plf-f&src=s&sid=717b54d90bc8702e21dcef2c32528d2b&sot=b&sdt=b&sl=29&s=TITLE-ABS-KEY%283d+hernia+mesh%29&relpos=12&citeCnt=0&searchTerm=&featureToggles=FEATURE\\_NEW\\_MAIN\\_SECTION:1,FEATURE\\_NEW\\_SOURCE\\_INFO:1,FEATURE\\_NEW\\_REAXYS\\_SECTION:1,FEATURE\\_NEW\\_SCIVAL\\_TOPICS:1,FEATURE\\_VIEWS\\_COUNT:1](https://www-scopus-com.login.ezproxy.library.ualberta.ca/record/display.uri?eid=2-s2.0-85097081679&origin=resultslist&sort=plf-f&src=s&sid=717b54d90bc8702e21dcef2c32528d2b&sot=b&sdt=b&sl=29&s=TITLE-ABS-KEY%283d+hernia+mesh%29&relpos=12&citeCnt=0&searchTerm=&featureToggles=FEATURE_NEW_MAIN_SECTION:1,FEATURE_NEW_SOURCE_INFO:1,FEATURE_NEW_REAXYS_SECTION:1,FEATURE_NEW_SCIVAL_TOPICS:1,FEATURE_VIEWS_COUNT:1) (accessed May 27, 2021).
- [34] “PROLENE® Polypropylene Hernia System | J&J Medical Devices.” <https://www.jnjmedicaldevices.com/en-US/product/prolene-polypropylene-hernia-system> (accessed May 28, 2021).
- [35] “ULTRAPRO Hernia | Hernia System | J&J Medical Devices.” <https://www.jnjmedicaldevices.com/en-US/product/ultrapro-hernia-system> (accessed May 28, 2021).
- [36] D. S. Levi, N. Kusnezov, and G. P. Carman, “Smart materials applications for pediatric cardiovascular devices,” *Pediatric Research*, vol. 63, no. 5. Nature Publishing Group, pp. 552–558, May 2008, doi: 10.1203/PDR.0b013e31816a9d18.
- [37] Y. Dündar, R. A. Hill, A. Bakhai, R. Dickson, and T. Walley, “Angioplasty and stents in coronary artery disease: A systematic review and meta-analysis,” *Scandinavian Cardiovascular Journal*, vol. 38, no. 4. Taylor & Francis, pp. 200–210, 2004, doi: 10.1080/14017430410032325.
- [38] K. Rabe and H. Sievert, “Carotid artery stenting: State of the art,” *Journal of Interventional Cardiology*, vol. 17, no. 6. John Wiley & Sons, Ltd, pp. 417–426, Dec. 01, 2004, doi: 10.1111/j.1540-8183.2004.04085.x.

- [39] J. P. Cheatham, “Stenting of coarctation of the aorta,” *Catheter. Cardiovasc. Interv.*, vol. 54, no. 1, pp. 112–125, Sep. 2001, doi: 10.1002/ccd.1249.
- [40] L. L. Stepan, D. S. Levi, and G. P. Carman, “A thin film nitinol heart valve,” *J. Biomech. Eng.*, vol. 127, no. 6, pp. 915–918, Nov. 2005, doi: 10.1115/1.2049311.
- [41] Q. Meng and J. Hu, “A review of shape memory polymer composites and blends,” *Composites Part A: Applied Science and Manufacturing*, vol. 40, no. 11, pp. 1661–1672, Nov. 2009, doi: 10.1016/j.compositesa.2009.08.011.
- [42] H. Meng and G. Li, “A review of stimuli-responsive shape memory polymer composites,” *Polymer*, vol. 54, no. 9, Elsevier Ltd, pp. 2199–2221, Apr. 19, 2013, doi: 10.1016/j.polymer.2013.02.023.
- [43] M. Zarek, M. Layani, I. Cooperstein, E. Sachyani, D. Cohn, and S. Magdassi, “3D Printing of Shape Memory Polymers for Flexible Electronic Devices,” *Adv. Mater.*, vol. 28, no. 22, pp. 4449–4454, Jun. 2016, doi: 10.1002/adma.201503132.
- [44] W. M. Huang, B. Yang, and Y. Q. Fu, *Polyurethane shapememory polymers*. CRC Press, 2011.
- [45] M. L. Auad, V. S. Contos, S. Nutt, M. I. Aranguren, and N. E. Marcovich, “Characterization of nanocellulose- reinforced shape memory polyurethanes,” *Polym. Int.*, vol. 57, no. 4, pp. 651–659, Apr. 2008, doi: 10.1002/PI.2394.
- [46] “[PDF] Shape Memory Materials for Biomedical Applications | Semantic Scholar.” <https://www.semanticscholar.org/paper/Shape-Memory-Materials-for-Biomedical-Applications-Feninat-Laroche/59db9866d029312f3577b6e9b62a7e295dc319cc> (accessed Jun. 18, 2021).
- [47] M. Behl and A. Lendlein, “Shape-memory polymers,” *Mater. Today*, vol. 10, no. 4, pp. 20–28, Apr. 2007, doi: 10.1016/S1369-7021(07)70047-0.
- [48] “(4) (PDF) Medical applications of shape memory polymers.” [https://www.researchgate.net/publication/5319248\\_Medical\\_applications\\_of\\_shape\\_memory\\_polymers](https://www.researchgate.net/publication/5319248_Medical_applications_of_shape_memory_polymers) (accessed Jun. 18, 2021).
- [49] M. F. Metzger, T. S. Wilson, D. Schumann, D. L. Matthews, and D. J. Maitland, “Mechanical Properties of Mechanical Actuator for Treating Ischemic Stroke,” 2002.
- [50] H. M. Wache, D. J. Tartakowska, A. Hentrich, and M. H. Wagner, “Development of a polymer stent with shape memory effect as a drug delivery system.”

- [51] M. M. Zimkowski, M. E. Rentschler, J. A. Schoen, N. Mandava, and R. Shandas, “Biocompatibility and tissue integration of a novel shape memory surgical mesh for ventral hernia: In vivo animal studies,” *J. Biomed. Mater. Res. - Part B Appl. Biomater.*, vol. 102, no. 5, pp. 1093–1100, Jul. 2014, doi: 10.1002/jbm.b.33091.
- [52] Y. Chen, I. T. Garces, T. Tang, and C. Ayranci, “Cellulose nanocrystals reinforced shape memory polymer cardiovascular stent,” *Rapid Prototyp. J.*, vol. 27, no. 1, pp. 37–44, Jan. 2021, doi: 10.1108/RPJ-01-2020-0019.
- [53] “(No Title).” [https://www.insightra.com/wp-content/uploads/2019/01/PROFLOR\\_patient\\_info-1.pdf](https://www.insightra.com/wp-content/uploads/2019/01/PROFLOR_patient_info-1.pdf) (accessed May 31, 2021).
- [54] R. Firoozabadi, P. Stafford, and M. Routt, “Risk of spermatic cord injury during anterior pelvic ring and acetabular surgery: An anatomical study,” *Arch. Bone Jt. Surg.*, vol. 3, no. 4, pp. 269–273, 2015, doi: 10.22038/abjs.2015.4303.
- [55] I. T. Garces, S. Aslanzadeh, Y. Boluk, and C. Ayranci, “Effect of moisture on shape memory polyurethane polymers for extrusion-based additive manufacturing,” *Materials (Basel)*, vol. 12, no. 2, Jan. 2019, doi: 10.3390/ma12020244.
- [56] T. Kim and Y. G. Lee, “Shape transformable bifurcated stents,” *Sci. Rep.*, vol. 8, no. 1, p. 13911, Dec. 2018, doi: 10.1038/s41598-018-32129-3.
- [57] J. Villacres, D. Nobes, and C. Ayranci, “Additive manufacturing of shape memory polymers: effects of print orientation and infill percentage on mechanical properties,” *Rapid Prototyp. J.*, vol. 24, no. 4, pp. 744–751, May 2018, doi: 10.1108/RPJ-03-2017-0043.
- [58] U. Klinge, J. Conze, W. Limberg, C. Brücker, A. P. Öttinger, and V. Schumpelick, “Pathophysiologie der bauchdecken,” *Chirurg*, vol. 67, no. 3, pp. 229–233, Mar. 1996, Accessed: Jun. 04, 2021. [Online]. Available: <https://europepmc.org/article/med/8681695>.
- [59] C. N. Brown and J. G. Finch, “Which mesh for hernia repair?,” *Annals of the Royal College of Surgeons of England*, vol. 92, no. 4. Royal College of Surgeons of England, pp. 272–278, May 2010, doi: 10.1308/003588410X12664192076296.
- [60] S. Roman, N. Mangir, L. Hympanova, C. R. Chapple, J. Deprest, and S. MacNeil, “Use of a simple in vitro fatigue test to assess materials used in the surgical treatment of stress urinary incontinence and pelvic organ prolapse,” *Neurourol. Urodyn.*, vol. 38, no. 1, pp. 107–115, Jan. 2019, doi: 10.1002/nau.23823.

- [61] P. P. Pott, M. L. R. Schwarz, R. Gundling, K. Nowak, P. Hohenberger, and E. D. Roessner, “Mechanical Properties of Mesh Materials Used for Hernia Repair and Soft Tissue Augmentation,” *PLoS One*, vol. 7, no. 10, Oct. 2012, doi: 10.1371/journal.pone.0046978.
- [62] S. Roman, N. Mangir, L. Hympanova, C. R. Chapple, J. Deprest, and S. MacNeil, “Use of a simple in vitro fatigue test to assess materials used in the surgical treatment of stress urinary incontinence and pelvic organ prolapse,” *Neurourol. Urodyn.*, vol. 38, no. 1, pp. 107–115, Jan. 2019, doi: 10.1002/nau.23823.